DEVELOPMENT OF CuO-ZnO COMPOSITE NANOMATERIALS FOR POTENTIAL APPLICATION IN DYE DEGRADATION

Dissertation submitted

In partial fulfilment of the requirements of the degree of

Master of Technology

In

BIOPROCESS ENGINEERING

By

SANDEEP KUMAR JENA

(Enrolment No: 16556007)

Under the supervision of

Dr. P. GOPINATH

DEPARTMENT OF BIOTECHNOLOGY

INDIAN INSTITUTE OF TECHNOLOGY ROORKEE

ROORKEE - 247667 (INDIA)

MAY, 2018

CANDIDATE'S DECLARATION

I hereby declare that the work presented in dissertation entitled "**DEVELOPMENT OF CuO-ZnO COMPOSITE NANOMATERIALS FOR POTENTIAL APPLICATION IN DYE DEGRADATION**" submitted in partial fulfilment of the requirements for the award of degree of Master of Technology in Bioprocess Engineering, Indian Institute of Technology Roorkee, is an authentic record of my work carried out under the supervision of **Dr. P. Gopinath**, Associate Professor, Department of Biotechnology, IIT Roorkee. The matter embodied in this has not been submitted by me for the award of any other degree.

Sandeep Kumar Jena
Enrolment No. 16556007
Date:

CERTIFICATE

This is to certify that the above statement made by the candidate is correct to the best of my knowledge.

Dr. P.Gopinath
Supervisor
Associate Professor
Department of Biotechnology
Indian Institute of Technology Roorkee

ACKNOWLEDGEMENTS

It is with my deepest sense of application that I express my foremost acknowledgement and sincere thanks to my supervisor **Dr. P. Gopinath**, Associate Professor, Department of Biotechnology, Indian Institute of Technology Roorkee, for believing in my ability and continuous care, support as well as valuable guidance throughout my work. Without his immense support and motivation, this endeavour of mine would not have been successful. Working under his guidance was a privilege and an excellent learning experience that I will cherish forever.

I sincerely thankful to my mentor **Raj Kumar Sadasivam**, Ph. D scholar for his immense support and guidance throughout the entire dissertation work. Also I acknowledge my dear friend **Palak Gupta** for her precious time and continuous support in completing the thesis.

This is dedicated to my beloved parents **Mr. Rajendra Jena** and **Mrs. Aruna Jena** and my dear siblings for their continuous love and encouragement. I thank the almighty for his eternal and everlasting blessings.

I owe a depth of gratitude to **Dr. A. K Sharma**, H.O.D, Department of Biotechnology and also the Institute instrumentation centre (IIC), Department of Chemistry and MMED are sincerely acknowledged for providing various analytical facilities.

Sandeep Kumar Jena

ABSTRACT

The photocatalytic efficiency of as-prepared CuO-ZnO composite nanomaterials were investigated towards degradation of congo red (CR) dye in presence of visible light with complete mineralization into less toxic CO_2 and water. Herein, Cuo-ZnO composite nanomaterials have been fabricated by electrospinning followed by heat treatment methods i.e. hydrothermal and calcination. The products were characterized using X-Ray Diffraction (XRD), Fourier Transform Infra Red (FTIR), Thermo Gravimetric Analysis (TGA), Transmission Electron Microscope (TEM) and X-Ray Spectroscopy (XPS) for their morphological and structural details. The photocatalytic experiments were conducted for degradation of CR dye under solar irradiation. It was found that photocatalytic reaction followed pseudo first order kinetics from which the rate constants were determined. The experimental results revealed calcined sample showed higher photocatalytic activity in degradation of CR dye as compared to hydrothermally treated sample. This increased efficiency was ascribed to better separation of excited electrons and holes due to development of a p-n heterojunction at the interface of the p-type (CuO) and n-type (ZnO) semiconductors. Photoluminescence studies (PL) were performed to explore separation/recombination rate of photogenerated charge carriers. The optical properties of samples were analyzed using UV-Visible NIR spectroscopy. Finally, the reusability studies were carried out up to ten cycles to evaluate stability and viability of multiple utilizations of photocatalysts in the degradation of CR dye. These results unfolded the immense potential of as-prepared CuO-ZnO composite nanomaterials so they can be implemented persistently and efficiently in water remediation in industry.

Keywords: Electrospinning, CuO, ZnO, hydrothermal, calcination, photocatalysis, congo red (CR) dye

S. No

TABLE OF CONTENTS

Page No

Figure No	LIST OF FIGURES	Page No

Table No	LIST OF TABLES	Page No

ABBREVIATIONS AND SYMBOLS

%	Percentage
θ	Theta
λ_{ex}	Excitation wavelength
λ_{em}	Emission wavelength
µg	Microgram
µL	Microlitre
°C	Degree Celsius
h^+	Free holes
Å	Angstrom
a.u	Arbitrary unit
2D	Two-dimensional
3D	Three-dimensional
k	first order rate constant
cm	Centimeter
C_0	Concentration at 0 min
CO_2	Carbon dioxide
CB	Conduction band
CR	Congo red
C_t	Concentration at time t
CuAc	Copper actetate monohydrate
Cu	Copper
CuO	Copper oxide
DI	Deionized water
R	Diffuse reflectance
DRS	Diffuse reflectance spectroscopy
eV	Electron volt
EDX	Energy dispersive X-ray spectrometry
E_g	Band gap energy

DMF	Dimethylformamide
FE-SEM	Field emission scanning electron microscopy
FTIR	Fourier transform infrared spectroscopy
h	Hour
HR-TEM	High resolution transmission electron microscope
H_2	Hydrogen
OH	Hydroxyl group
JCPDS	Joint committee on powder diffraction standards
kV	Kilo volts
F(R)	Kubelka monk function
L	Litre
m	Mass
mg	Milligram
mL	Millilitre
min	Minute
M_W	Molecular weight
nm	Nanometer
N	Nitrogen
O_2	Oxygen
PPM	Parts per million
hν	Photon energy
PAN	Polyacrylonitrile
KBr	Potassium bromide
PL	Photoluminescence
Rpm	Revolutions per minute
SAED	Selected area diffraction pattern
TGA	Thermogravimetric analysis
UV	Ultraviolet
VB	Valence band
H_2O	Water
Cm^{-1}	Wavenumber
Wt %	Weight percentage

XPS	X-Ray photoelectron spectroscopy
XRD	X-Ray diffraction
ZnO	Zinc oxide

CHAPTER 1
INTRODUCTION

Introduction

With ever increasing industrialization and urbanization, the environment as well as water gets hugely polluted[1]. Nowadays, the adulteration of water with multiple pollutants such as pesticides, bacterial pathogens, heavy metal ions and synthetic organic dyes is globally becoming an environmental catastrophe[2]. Among these, organic dyes (methelene blue, methelene orange, congo red etc.) and bacterial pathogens (*Staphylococcus aureus, E coli* etc.) as they generate toxic secondary byproducts which are further nondegradable are extremely harmful pollutants present in water[3]. In addition to, some of the heavy metal ions that gets released from industrial effluents due to everyday usages such as As2+, Cd2+, Co2+, Cu2+ Hg2+ and Pb2+ are deleterious not only to aquatic life but also to human health through consumption of contaminated aquatic species[4]. Reports suggest that nearly 10,000 of different commercial dyes are known, with worldwide annual production of over 7×10^5 tons[5]. These dyes are highly toxic and not easily get mineralized under natural environmental conditions as most of the dyes are azo dyes contain chromophoric azo group (-N=N-). Furthermore, they are recalcitrant and carcinogenic in nature cause miscellaneous cancers[6,7]. While scores of technologies have emeged for water remedition such as membrane filtration, flocculation, ozonation, electrodialysis , electrochemical treatment etc., but none of these are reliable, cost effective and efficient technology[8–10]. Therefore, photocatalysis has recently attracted more attention as a promising technique for resolving environmental issues mostly in the deterioration of organic pollutants in water remediation[11]. As it leads to mineralization of toxic organic contaminants into less toxic carbon dioxide and water. Besides, it is eco-friendly, cost effective and bypasses the energy consumption utilizing naturally available solar light[12]. Hence, metal oxide based photocatalytic degradation has been unraveled as one of the most dynamic techniques to mitigate water related concerns[13,14].

Today, nanotechnology has amassed stupendous attention for their implementation in environmental remediation and pollution control because of their high surface area to volume ratio and have supreme physical and chemical properties[15,16]. Metal oxides (such as CuO, TiO_2, CeO_2, ZnO_2, SnO_2 , NiO, V_2O_5) play vital role in photocatalysis because of their band gap values, unique arrangement of electronic structure, light absorption properties and charge transport characteristics. Moreover, metal oxides are easily available in nature, biocompatible and capable of generating photoexcited charge carriers. Nevertheless, this approach still suffers from some limitations i.e. the fast recombination rate of photogenerated electrons and holes. In this case, excitation of electrons from conduction band to valence band upon UV irradiation (due to high bandgap value) not only increases the cost of water remediation but also precludes the utilization of easily available solar irradiation. To beat aforementioned issues, p-n junctions can be built in photocatalyst that lead to development of potential gradient which eases the separation of electrons and holes. Till date, myriads of mixed metal oxides and nanocomposites have been developed with desired morphologies and chemical properties.

In our present study, we synthesized CuO-ZnO mixed metal oxides nanofibrous membrane as CuO is favorable to use p-n junction-mediated photocatalytic degradation of organic dyes because of its narrow band gap value (Eg = 1.3 eV), abundant in nature, nontoxicity and p-type semiconducting properties whereas ZnO to coupled with CuO has high band gap value (Eg = 3.3 eV) and n-type semiconducting properties to develop potential gradient, hence to enhance photocatalytic efficiency. These nanofibrous membranesfind huge potential in photocatalytic application like degradation of synthetic dyes predominantly azo dyes. One more advantage is that their easy retrieval from treated solution without leaving any toxic secondary residues as well as retaining the same molar mass lacking any disintegration. These potential features of prepared-photocatalyst foster their application in industrial level for efficient removal of noxious organic pollutants present in waste water.

1.1 Objectives

The key objectives of this study are

- Fabrication of PAN-based metal oxide nanofibrous composites by coupling electrospinning technique followed by calcination and hydrothermal treatment.
- Characterization of nanofibrous composites using various analytical techniques.
- Investigation of dye degradation efficiency under visible light irradiation.
- Comparative analysis of photodegradation efficiency of as-prepared nanofibrous composites by calcination and hydrothermal technique.
- Reusability study in subsequent cycles of degradation reaction.

1.2 Significance of the present study

- A novel polymer PAN based fabrication of two dimensional CuO-ZnO nanofibrous composites using simple and cost effective electrospinning technique followed by post calcination and hydrothermal treatment.
- Photocatalytic efficiency of as-prepared nanofibrous composites towards CR dye under solar irradiation was investigated.
- Initially some control experiments were conducted to unveil the requirement of both photocatalyst and sun light for photocatalytic degradation.
- Kinetic studies were carried out to validate the experimental data as well as rate of photocatalysis.
- The complete mechanism of CR dye degradation under solar irradiation was explained.
- Photoluminescence (PL) studies were conducted to investigate recombination/separation rate of charge carriers.
- Reusability studies were performed to evaluate viability of photocatalysts for multiple cycles.

CHAPTER 2
REVIEW OF LITERATURE

2.1 Fabrication of nanofibers

Over the past few decades, there has been vast improvement in development of one dimensional (1D) nanostructures such as nanofibers, nanotubes, nanowires etc[17]. Nanofibers are one dimensional nanostructures having diameter of few hundred nanometer (less than 100 nm). Nanofibers have some unique properties that set apart from other nanostructures such as enhanced surface area to volume ratio and greater porosity in different applications like water purification process[18], solar photocatalytic degradation[19], biosensor[20], tissue scaffold in tissue engineering[21], and drug delivery etc[22].

In general, there are three methods available for the fabrication of nanofibers i.e. self assembly[23], phase separation[24] and electrospinning[25]. Self assembly is a phenomenon in which atoms or molecules of a system come together to form a larger functional unit where intermolecular force leads to spontaneous gathering of components into stable nanostructure[26] whereas in phase separation technique, solvent rich phase and polymer rich phase get separated by thermal energy or by introducing the non-solvent into polymer phase in non-solvent induced phase separation. It provides many advantages such as simple, energy efficient and cost effective but it has one drawback that it can't be scaled up for laboratory purpose. Nanofibers with diameter of 50- 500 nm can be fabricated using phase separation technique[27,28].

The third technique is electrospinning which is more advanced and vastly used in the fabrication continous ultrafine nanofibers of few nanometers. The term "electrospinning" was derived from "electrostatic forces" which ease the fabrication of ultrathin nanofibers when a high voltage is applied[29]. Electrospinning is an old technique was first patented by J.F. Cooley in 1900 and W.J. Morton in 1902[30]. A couple of patents issued by Formhals (1934-1944) demonstrating the set up of electrospining and drawing of nanofibers applying electrostatic forces. In addition to, Antonin Formhlas in 1934 filed a patent on electrospinning for the generation of textile yarns and for

electrospinning cellulose acetate using acetone and monomethyl ether of ethylene glycol as solvents[31,32]. This electrospinning renders numerous advantages over other techniques as it facilitates the fabrication of nanofibers of few nanometers with high porosity, enhanced surface area to volume ratio, malleability and the ability to control the composition of nanofibers. With these additional supremacies, ultrathin electrospun nanofibers have been successfully implanted in countless fields such as photocatalysis, tissue engineering scaffolds, water filtration, healthcare, pharmaceutical, optical sensor, optical electronics, defense, biotechnology and environmental engineering etc[33–36]. Overall, this is a very simple and robust technique to engineer nanofibers from a wide variety of polymers.

2.2 Principle of electrospinning

Electrospinning, an electrostatic fiber fabrication technique, uses electrostatic forces to generate ultrathin fibers from polymer solutions or melts in the range of several tens of kvs. The process of electrospinning is a major focus of attention in recent years not only due to its flexibility in spinning a wide variety of polymeric fibers but also due to its ability to produce ultrathin and continous fibers on a scale of nanometers that is otherwise difficult to achieve by using any standard technologies. Electrospinnig set up is very simple and consists of three major components such as high voltage supply, spinneret with syringe and grounded collector.

In electrospinning, a polymer solution is held by its surface tension at the end of capillary tube. When a high voltage is applied, charge is uniformly distributed over the surface of droplet coming out of the nozzle. The droplet is now introduced to two electrostatic forces i.e. electric charge induced on the liquid surface and Coloumbic force due to external electric field. The electrostatic repulsion between charges on the surface and the external field results in the morphological change in the droplet from pendant to conical shape known as taylor cone. When increasing voltage exceeds threshold point where repulsive electrostatic force dominates surface tension resulting in inversion of rounded tip and ejection of charged jet from taylor cone. In the meantime, solvent present in polymer solution evaporates leaving behind the nanofibers on the metallic collector. Sometimes problem may occur that the tip of needle gets blocked due to hydrolysis, condensation and gelation of precursor solution resulting in fabrication of nonuniform fibers. The problem can be surpassed by changing precursor or by adding suitable catalyst to adjust hydrolysis or gelation rate[37]. In addition to, there are several

other parameters that can be considered to control morphology and diameter of nanofibers[38,39]. These parameters are categorized into three groups:

Table 2.1 Various parameters of electrospinning

Solution	Processing parameters	Atmosphere
Viscocity	Voltage applied	Temperature
Surface tension	Flow rate	Humidity
Conductivity	Distance between spinneret and collector	
Elasticity		
Solvent properties		
Solution concentration		

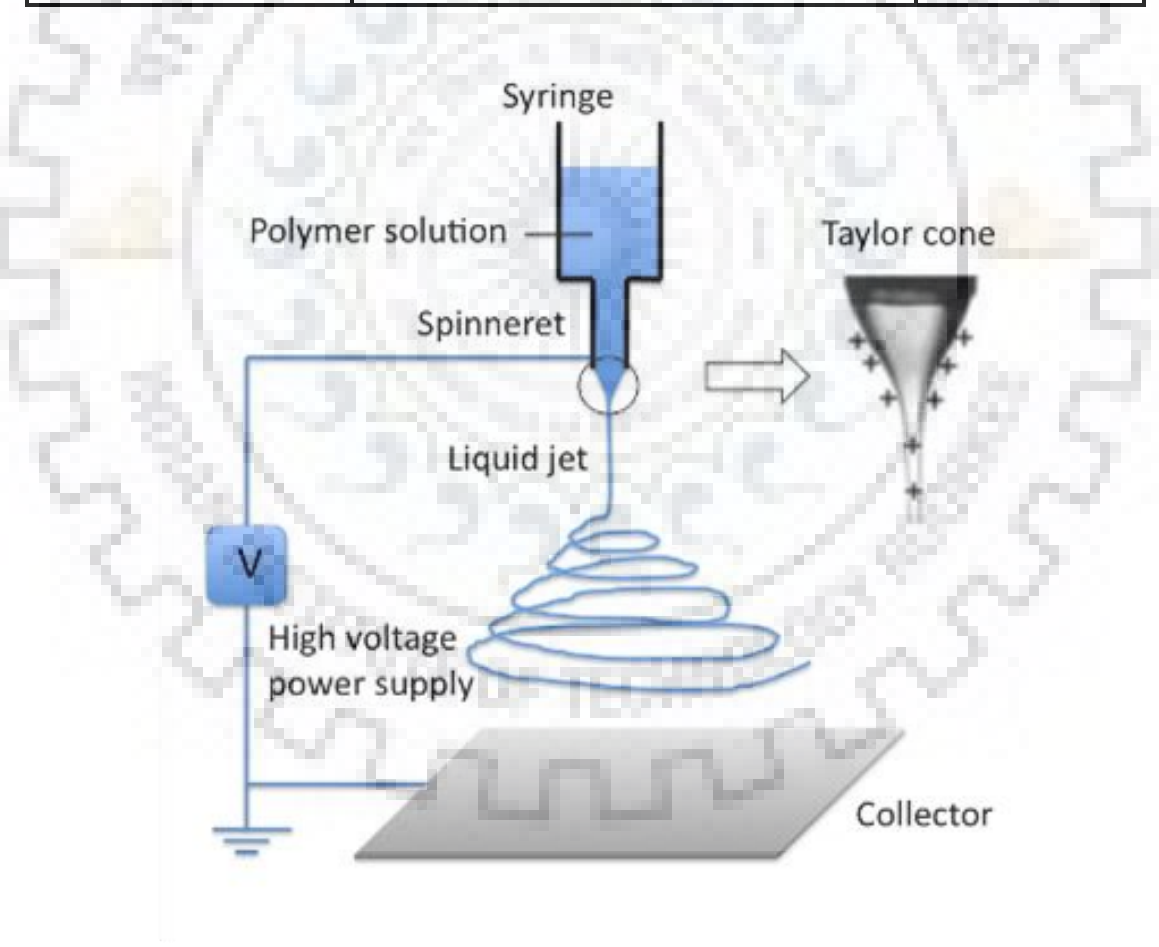

Figure 2.1 Schematic diagram of electrospinning for the fabrication of ultrathin nanofibers

2.3 Congo red

In our present work, congo red (CR) dye was taken as model dye for photocatalytic experiments. CR dye is an organic dye, the sodium salt of 3,3′-([1,1′-biphenyl]-4,4′-diyl)bis(4-aminonaphthalene-1-sulfonic acid. It is an azo dye characterized by two nitrogen to nitrogen double bonds (-N=N-) that are usually attached to benzene and naphthalene rings[40]. When it is used as photocatalyst, the azo bonds are oxidized by free hydroxyl radicals or holes or reduced by electrons. The cleavage of azo bonds eases the degradation of CR dye. It is used as pH indicator as it can change color from blue to red at pH 3 to 5.2. The color of azo dyes is determined by the number of azo bonds present and the nature of chromophores and auxochromes attached[27]. So when it is dissolved in water, it leads to formation of red colloidal solution. It finds use in molecular biology laboratories for staining purposes. It is highly noxious because of its caricinogenic component (i.e. benzidyne). It invites skin irritation and has dreadful effects on respiratory system and reproductive system of human body[41].

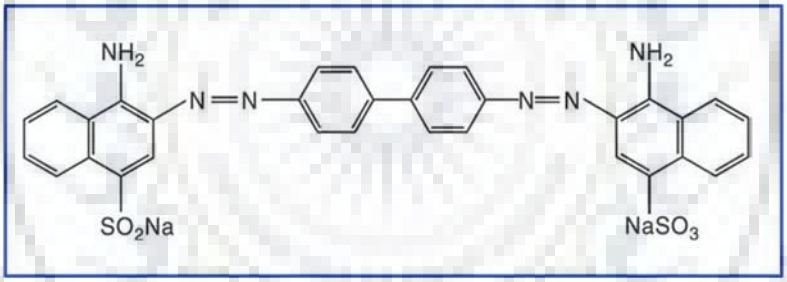

Figure 2.2 Molecular structure of CR dye

2.4 Hydrothermal method

Hydrothermal synthesis is a very simple and fascinating technique to generate various metal oxide nanostructures such as nanoparticles[42], nanofibrous membrane[43], nanorods[44], nanoflowers[45] and nanowiresetc[46]. It is a heterogeneous reaction which occurs in the presence of aqueous solvent (eg. water, NaCl, H_2SO_4, KCl etc) under constant pressure and temperature in a closed environment for a certain time period. In this technique, several parameters such as type of solvent, surfactant, pH, temperature, pressure, reaction time and metal precursor salts etc have great contribution to shape the morphology and physio-chemical properties of nanostrucutures[47].

It provides the luxury of lower reaction temperature, increased purity, uniform anatomy, homogenous phase, crystallinity and mitigation of agglomeration of particles.

2.5 Calcination method

Calcination is a heating treatment to synthesis diverse metal oxides from metal precursor salts such as Fe_2O_3, CuO, Al_2O_3, NiO, MnO_2 and Cr_2O_3 etc[48]. The calcination temperature and heating rate have tremendous effects on morphology, structure, growth, surface property, porosity and especially photocatalytic effects of metal oxides[49]. Lingling He and Zhifang Tona prepared ZnO nanorods with heating rate 1° C/min at 300° C revealed best photocatalytic activity because of high oxygen vacancies and its distinctive one dimensional morphology[50].

2.6 Metal oxides

2.6.1 Copper oxide

Copper is an essential element having good thermal conductivities and high electrical properties. Its oxides such as CuO (monoclinic) and Cu_2O (cubic) are used as potential photocatalysts for organic dye degradation in presence of solar irradiation. CuO and Cu_2O are P-type semiconductor materials exhibiting narrow band gap of 1.9 to 2.1 eV and 2.1 to 2.6 eV respectively[51]. Copper oxide finds its application in chemical sensors, optical devices, photovoltaic cells and solar cells etc[52].

2.6.2 Zinc oxide

Zinc oxide (ZnO) is a wide band gap (3.3 eV) n-type semiconductor. ZnO has multifarious promising properties such as wide band gap, high electron mobility and good luminescence etc[53]. These favorable properties of ZnO set it apart from other metal oxides for various applications for light-emitting diodes, thin film transistors, transparent electrodes and photocatalysts etc.

Metal oxides are employed as photocatalysts because of their high porosity, unique electronic configuration and light absorption properties etc[54]. Besides, these are eco-friendly, abundant in nature, highly stable and able to generate photoexcited charge carriers which ease the photocatalytic degradation of organic dyes[55]. To increase the light absorption capacity and photocatalytic efficiencies, sometimes CuO and ZnO are coupled to form a p-n heterojunction[56].

2.7 Photocatalytic mechanism

When an n-type semiconductor is integrated with p-type semiconductor, a p-n heterojunction is developed. As a result, electrons from n-type diffuse to p-type semiconductor and holes drift to from p-type to n-type semiconductor till the system achieves equilibrium. So it leads to developing an electric field at junction of p-n semiconductors. When a light of certain threshold energy incident on heterojunction, the excited electrons drift towards conduction band of n-type semiconductor and vacant holes migrate towards valence band of p-type semiconductor. The electrons at the surface react with dissolved oxygen to produce superoxide radical ions ($O_2^{\cdot -}$) which finally gives rise to hydroxyl radicals ($OH^{\cdot}$) via generation of hydroperoxy radicals ($HO_2^{\cdot}$). Meanwhile holes are confined by water molecules on the top of catalyst to generate hydroxyl radicals ($OH^{\cdot}$), which facilitates degradation of organic dyes. The photocatalytic mechanism carried out by heterostructures demonstrated as follows:

$$\text{p-n heterostructure} + h\nu \rightarrow (e^-)\text{n-type} + (h^+)\text{p-type} \quad (1)$$

$$e^- + O_2 \rightarrow O_2^{\cdot -} \quad (2)$$

$$O_2^{\cdot -} + H_2O \rightarrow HO_2^{\cdot} + OH^- \quad (3)$$

$$HO_2^{\cdot} + H_2O \rightarrow H_2O_2 + OH^{\cdot} \quad (4)$$

$$H_2O_2 \rightarrow 2OH^{\cdot} \quad (5)$$

$$h^+ + OH^- \rightarrow OH^{\cdot} \quad (6)$$

Besides, while using visible light as a source of energy, it sometimes fosters to dye sensitization mechanism. The dye is sensitized when sunlight incident on it, as a result it drives excited electron into conduction band of metal oxide. These electrons react with ambient oxygen to yield free radicals which incorporate with the excited dye molecules to decompose them. The dye sensitization mechanism carried out by metal oxide as shown by equations below.

$$h^+ + H_2O \rightarrow OH^{\cdot} + H^+ \quad (7)$$

$$Dye + h\nu \rightarrow Dye^* \quad (8)$$

$$Dye^* + \text{heterostructure} \rightarrow Dye^{\cdot+}\text{heterostructure} + e_{CB}^- \quad (9)$$

$$e_{CB}^- + O_2 \rightarrow O_2^{\cdot-} \quad (10)$$

$$Dye^{\cdot+} + O_2^{\cdot-} \rightarrow \text{degradation products} \quad (11)$$

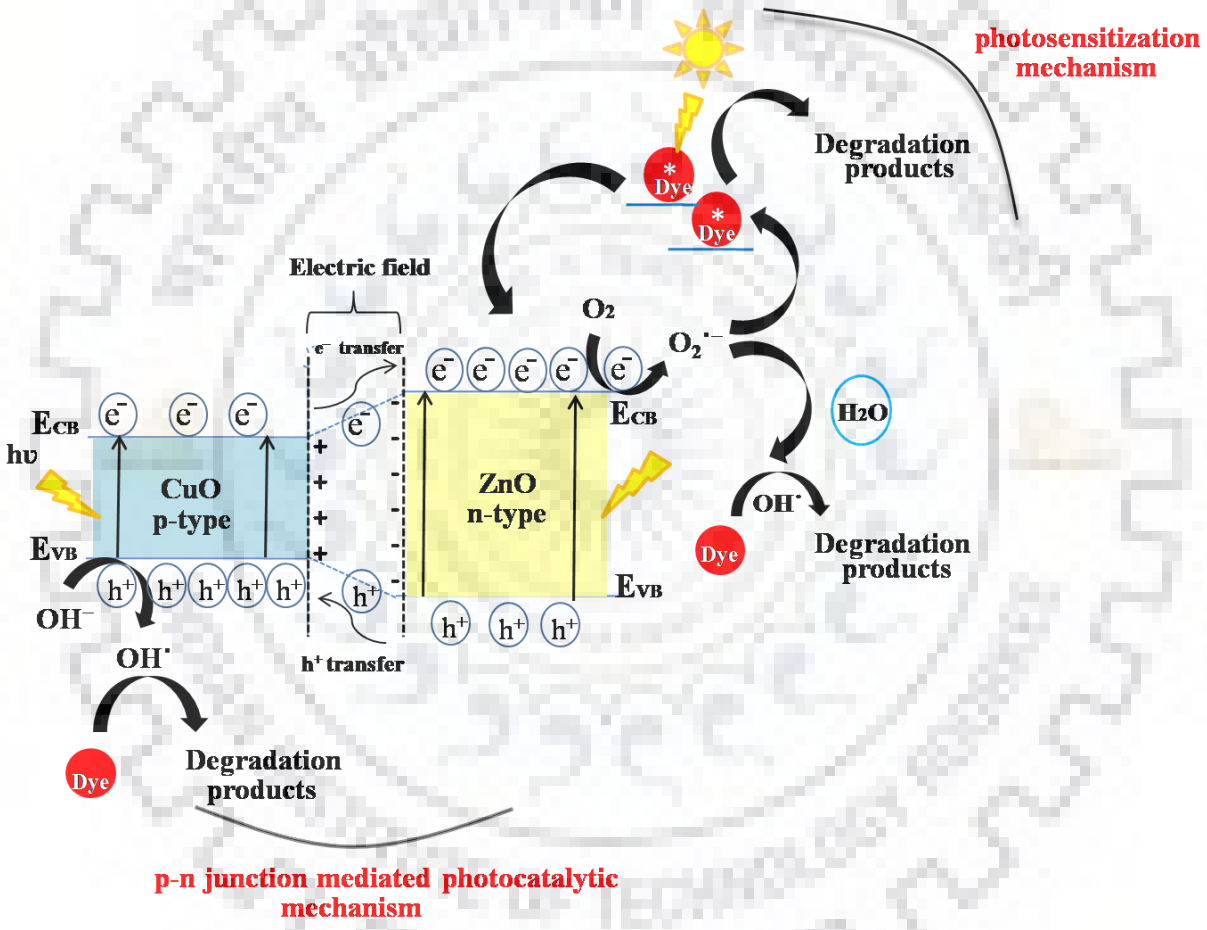

Figure 2.3 Different mechanisms of CR dye degradation in presence of sun light

CHAPTER 3
MATERIALS AND METHODS

3.1 Materials

3.1.1 Reagents

- Congo Red (CR)(Mw = 696.68 g/mol)
- Copper acetate monohydrate ($CuAc_2$) [$Cu(CH_3COO)_2 . H_2O$] (Mw = 199.65 g/mol)
- N, N- Dimethylformamide (DMF) [C_3H_7NO] (Mw = 73.09 g/mol)
- Polyacrylonitrile (PAN) [$(C_3H_3N)n$] (Avg. Mw = 150,000)
- Ultrapure Water (18 MΩ)
- Zinc acetate dihydrate ($ZnAc_2$) [$Zn(CH_3COO)_2 .2H_2O$] (Mw = 219.49 g/mol)

3.1.2 Equipments

- Autoclave (NANOMAG)
- Electrospinning machine (ESPIN NANO, PECO)
- Fourier transform infrared spectrometer (FTIR) (Thermo Nicolet)
- Thermogravimetric analyzer (TGA) (TG/DTA SII 6300 EXSTAR)
- Transmission electron microscope (TEM) (JEOL JEM-3200FS)
- Tube furnace (Nabertherm, Germany)
- UV–Visible spectrometer (Lasany double-beam L1 2800)
- UV-VIS-NIR spectrophotometer (PerkinElmer, LAMBDAL6020087)
- X-ray diffractometer (XRD) (Bruker AXS D8 Advanced)
- XPS (PHI 5000 VersaProbe III, Physical Electronics)

3.2 Methods

3.2.1 Preparation of CuAc/ZnAc/PAN polymeric blend solution

- Weighed 0.35 g (7 Wt%) of PAN (Polyacrylonitrile) and dissolved into 5 ml of DMF (N, N-Dimethylformamide) in two glass vials.
- The as-prepared aqueous solution was magnetically stirred at 350 rpm for 30 min at room temperature.
- Weighed 350 mg of copper acetate monohydrate (CuAc) and zinc acetate dihydrate (Zn Ac) and dissolved them into aqueous solution in two respective vials.
- **NOTE:** CuAc salt is dark green in color whereas the zinc acetate is colorless.
- Thereafter, copper acetate/PAN mixture was added slowly to the zinc acetate/PAN mixture and undergoes constant magnetic stirring for 12 h to get a homogenous green colored copper acetate/zinc acetate/PAN blend polymer solution (with molar ratio of Cu: Zn =1:1).

3.2.2 Fabrication of PAN/CuO-ZnO composite nanofibrous membrane

- The green viscous solution was filled in a 2.5 mL syringe with a metal needle and kept at a distance of 20 cm from the collector covered with the aluminium foil
- The flow rate of the solution was set at a rate of 0.45 mL/h and a fixed voltage of 12 kV was maintained between the needle tip and the grounded collector.
- After few hours, the nanofibrous sheet deposited on aluminium foil which was then taken and kept for heat treatment i.e. hydrothermal treatment at 200 ℃ for 12 h and calcined at 400℃ for 2 h in the presence of air to obtain CuO-ZnO nanofibrous composite membrane.

3.3 Characterization techniques

3.3.1 X-Ray diffraction (XRD)

The X-Ray diffraction was carried out to find out crystalline nature and size using Brucker AXS D8 advanced powder X-ray diffractometer with Cu-Kα radiation of wavelength λ = 1.5404 Å in the range of 20° to 90° with a scan rate of 0.5°/min. The diffraction peaks were analyzed using PANalytical Expert Highscore Plus software.

3.3.2 Fourier transform infrared (FTIR) spectroscopy

FTIR spectroscopy of nanofibrous composites was performed by properly mixing small amount of samples with KBr pellets using Thermo Nicolet spectrometer in the range of 4000-400 cm-1.

3.3.3 Thermogravimetric analysis (TGA)

Thermogravimetric analysis (TGA) was performed by TG/DTA SII 6300 EXSTAR thermal analyzer by heating up to temperature 800 °C with a constant heating rate of 5°/min.

3.3.4 High resolution transmission electron microscopy (HR-TEM)

The transmission electron micrographs and selected area electron diffraction (SAED) patterns were obtained using JEOL JEM-3200FS Field Emission Electron Microscope working at 200 keV with machine resolution of 0.4 nm. The samples were prepared by sonication and dispersed a couple of drops onto the nonglossy surface of carbon-coated copper grids.

3.3.5 Diffuse reflectance spectroscopy (DRS)

The optical properties of the samples were examined by recording diffuse reflectance spectra (DRS) in the range of 250 nm to 800 nm using UV-VIS-NIR spectrometer (PerkinElmer, LAMBDAL6020087). The as-prepared samples were powdered with help of mortar and pestle and used for data acquisition.

.3.3.6 X-Ray photoelectron spectroscopy (XPS)

The chemical & electronic states and composition of as-prepared nanofibrous composites were studied by using X-ray photoelectron spectroscopy (XPS) by exposing the samples with X-ray beam (A1 1486 single X-ray beam) and the equipment possessing C_{10} gun with vaccum pressure of 3.75 x 10^{-14} to 3.75 x 10^{-10} torr with 20 min of time of detector acquisition. All the raw data obtained were plotted in Origin Pro 8.0 software.

3.3.7 UV-Visible spectroscopy

The ability to absorb sun light of the samples was inspected by UV-Visible spectroscopy. The dye solution was scanned in the wavelength range of 200-800 nm. The photocatalytic experiments were conducted with the help of UV-Visible spectrophotometer (Lasany double-beam L1 2800). The absorbance of dye solution was taken at characteristic wavelength (λ = 500 nm) at fixed interval time during 11a.m. to 5 p.m. The concentration of dye was calculated using calibration curve plotted between absorbance and known concentration of the dye.

3.3.8 Photoluminescence (PL) studies

Photoluminescence (PL) spectra of the samples were obtained with the help of fluorescence spectrophotometer which is equipped with xenon lamp. The as-prepared samples were sonicated and set for data acquisition. The emission spectra were recorded with excitation wavelength at 370 nm for both calcined and hydrothermal samples.

3.4 Photocatalytic studies

Congo red (CR) dye was used as model dye to evaluate photocatalytic activity of both the samples. The photocatalytic experiments were performed by adding catalyst, having different molar mass, in a dye solution with an initial concentration of 180 ppm (water 4.5 mL + dye 0.5 mL = 5 mL dye solution). The decrease in dye concentration was evaluated using a UV-visible double beam spectrophotometer by taking the absorbance at 500 nm at particular intervals of time. The percentage of dye left after a particular time interval was calculated as follows:

$$\% \text{ dye left after time at } t = (C_0/C_t) \times 100$$

Where, t is the time, C_0 denotes concentration of the initial solution and C_t, concentration after time t. All the sunlight mediated photocatalytic experiments as well as comparative studies were performed in between 11:00 a.m. and 5:00 p.m.

3.5 Reusability studies

Reusability study was performed up to ten cycles with the synthesized composite material, but with the fresh aqueous dye solution. After each cycle, the samples were washed with distilled water and used in same experimental conditions.

CHAPTER 4
RESULTS AND DISCUSSIONS

4.1 Synthesis of CuO-ZnO nanofibrous composites

Fabrication of CuO-ZnO nanofibrous composites was done using very simple, facile and cost effective electrospining technique followed by heat treatment i.e. calcination at 400° C for 2 hr and hydrothermal at 200°C for 12 hr. The metal precursor salts (copper and zinc) were dissolved in dimethylformamide (DMF) and then polyacrylonitrile (PAN) was added to prepare homogenous blend solution. The solution was then electrospun with a flow rate of 0.45 mL/h at a fixed voltage of 12 kV to fabricate ultrathin and continuous nanofibers which get deposited on collector plate in the form of nanosheet. The as-prepared thin sheet was peeled off and given heat treatment to obtain CuO-ZnO nanofibrous composites. The nanofibrous composites were employed as photocatalyst to degrade CR dye solution under visible light. The complete procedure was schematically represented in figure 4.1.

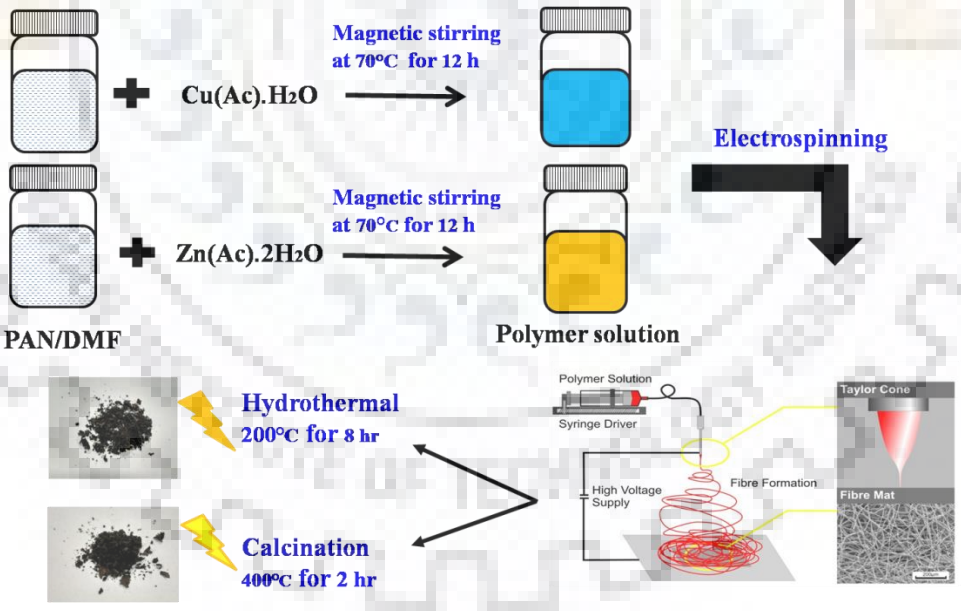

Figure 4.1 Schematic representation of fabrication of CuO-ZnO nanofibrous composites using electrospinning

4.2 X-ray diffraction (XRD) analysis

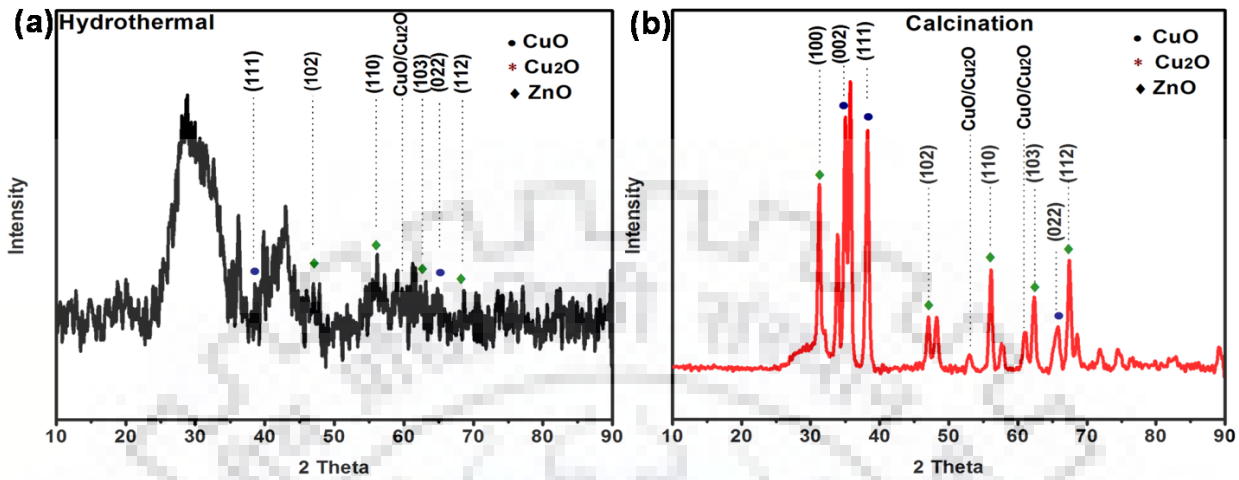

Figure 4.2 (a, b) XRD patterns of hydrothermal and calcined sample

The structural details and crystalline property of metal oxide PAN nanofibrous composites were analyzed by powder X-ray diffraction pattern (XRD) using PANalytical X'pert High Score Plus software. Figure 4.2(a, b) represent the typical XRD patterns of hydrothermally treated sample and calcined sample respectively where standard peaks of all metal oxides formed are observed. The characteristic diffraction peaks indexed to 2θ are 47.35 , 56.22 , 62.19 and 67.58° corresponding to (102), (110), (103) and (112) crystal planes respectively according to JCPDS card number 01-079-0208 which determines hexagonal structure of zinc oxide (ZnO). The high intense peaks observed at 38.48 and 65.85° related to planes (111) and (022) can be assigned to monoclinic phase of CuO (JCPDS no 00-048-1548) and some planes attributed to the cubic phase of Cu_2O (JCPDS no 00-002-1067) which confirms the complete oxidation of copper. The broad peaks found between 25 and 35° is due to the semi crystalline nature of PAN polymer. The crystallite size of metal oxide nanofibrous composites was also determined using the Debye Scherrer formula:

$$t = K\lambda / B\cos\theta$$

where t is the crystallite size , K is numeric constant of value 0.9 , λ is wavelength of Cu Kα radiation which is equal to 0.154 nm , B is full width at half maximum (FWHM). Using this above formula, the mean size of metal oxide nanofibrous composites was found to be 7.44 nm.

Table 4.1 Various parameters of XRD analysis

Sample name	Angle (2θ)	Crystal plane	JCPDS no	Crystal structure
ZnO	47.35 56.22 62.19 67.58	(102) (110) (103) (112)	01-079-0208	Hexagonal
CuO	38.48 65.85	(111) (022)	00-048-1548	Monoclinic
Cu_2O	N.A	N.A	00-002-1067	Cubic

4.3 Fourier transform infrared (FTIR) analysis

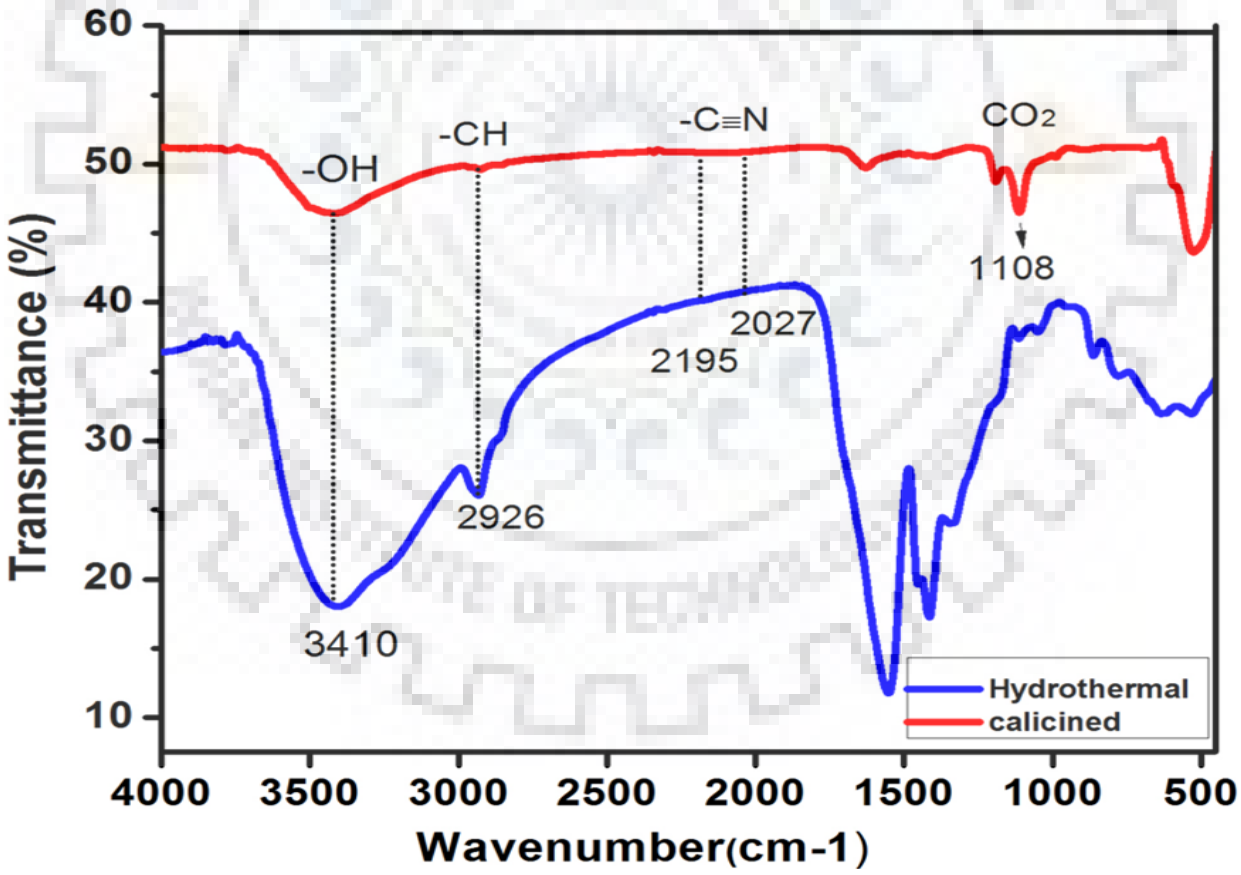

Figure 4.3 FTIR spectra for CuO-ZnO nanofibrous composites

Fourier transform infrared (FTIR) spectrum analysis was performed to find out functional groups present in CuO-ZnO nanofirous composites as-prepared by electrospinning followed by heat treatment techniques i.e. hydrothermal and calcination. A broad peak at 3400 cm^{-1} and 3410 cm^{-1} found as –OH stretching vibration which confirms the absorbed water molecules over the surface of nanofibrous composites in hydrothermal and calcination respectively.[57] A sharp peak at 2926 cm^{-1} depicts symmetric and antisymmetric stretching and bending vibrations of -CH group.[58] Tiny peaks discovered between 2195 cm^{-1} and 2027 cm^{-1}confirm the presence of nitrile group (-C≡N) of polyacrylonitrile (PAN) in nanofiber.[59]Additional peaks from 1622 cm^{-1} to 1326 cm^{-1} ascribed to stretching vibrations of –CH group both in hydrothermal and calcined sample. An intense peak tracked down at 1108 cm^{-1} shows absorbed CO_2 in calcination.[60] The characteristic spectra found from 861 cm^{-1} to 516 cm^{-1} indicate the formation of CuO and ZnO in both hydrothermal and calcinced samples.[61]

4.4 Thermogravimetric analysis (TGA)

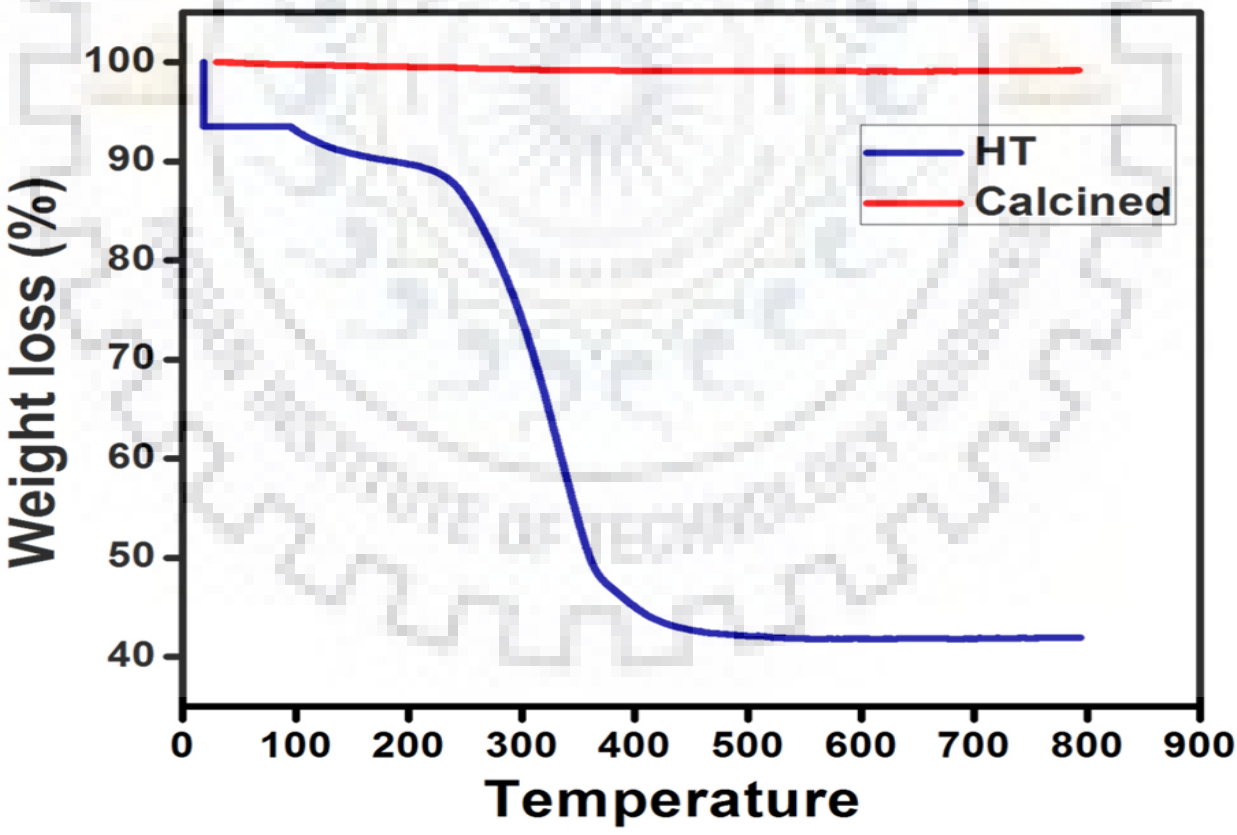

Figure 4.4 TGA patterns for CuO-ZnO nanofibrous composites

The thermogravimetric analysis (TGA) of CuO-ZnO nanofibrous composites was performed to study the thermal degradation behavior by measuring their change in mass as a function of temperature in a defined atmosphere. The nanofibrous composites follow the uniform degradation profile after hydrothermal treatment. The initial weight loss (less than 150°C) due to physiochemical absorption of moisture and low molecular weight solvents present in composites. Further it undergoes cleavage of C-C bonding in polyacrylonitrile (PAN) polymer between 150 and 250 °C and then undergoes (between 250 and 500°C) combustion of carbon present in nanofirous composites corresponds to 40 to 80% weight loss. Only 41 % residues left behind at the end of 800°C which confirms the thermal stability of CuO-ZnO nanofibrous composites whereas, in calcination 99% by weight of residues are left, which ascertained that the samples are thermally stable as compared to the samples synthesized by hydrothermal method. Moreover, in calcination process there is initial loss of weight could be due to the moisture and unreacted components.

4.5 High resolution - transmission electron microscopy (HR-TEM) analysis

The structural details and morphology of CuO-ZnO nanofibrous composites were analysed using transmission electron microscopy (TEM).

4.5.1 TEM analysis of hydrothermally treated sample

Figure 4.5(a, b) represents the HRTEM image of hydrothermal sample which is a single nanofiber due to the presence of PAN polymer, possesses the diameter of 450 – 500 nm approximately. The SAED pattern (inset the figure 4.5(c)) shows the amorphous nature of hydrothermal sample. Figure 4.6(a-g) depicts elemental mapping which confirms the existence of the elements carbon, oxygen and nitrogen in addition to copper and zinc. It clearly manifests the homogenous distribution of copper and zinc throughout the nanofibers overall. Figure 4.7 represents EDX analysis of hydrothermal sample revealed the presence of copper (11.96 Wt %) and zinc (10.92 Wt %) in almost equal amounts on the surface of nanofibers. As the spectrum contained five peaks corresponding to C, O, N, Cu and Zn, respectively which confirmed that no other impurities were detected.

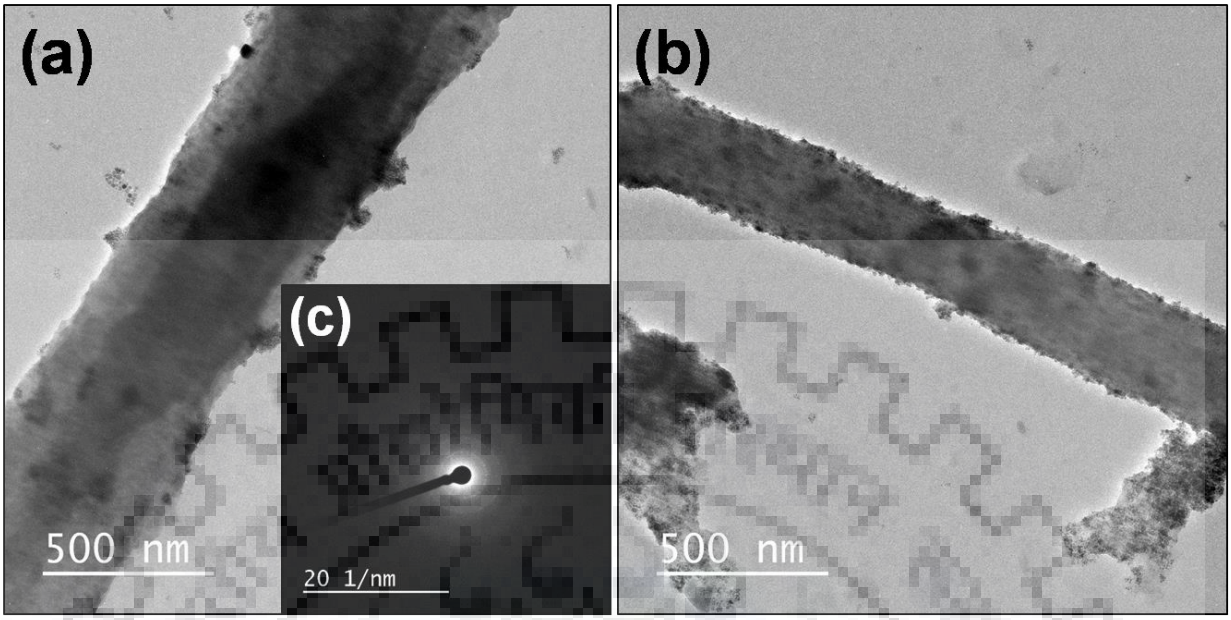

Figure 4.5(a-b) TEM images of hydrothermally treated sample, (c) its SAED pattern

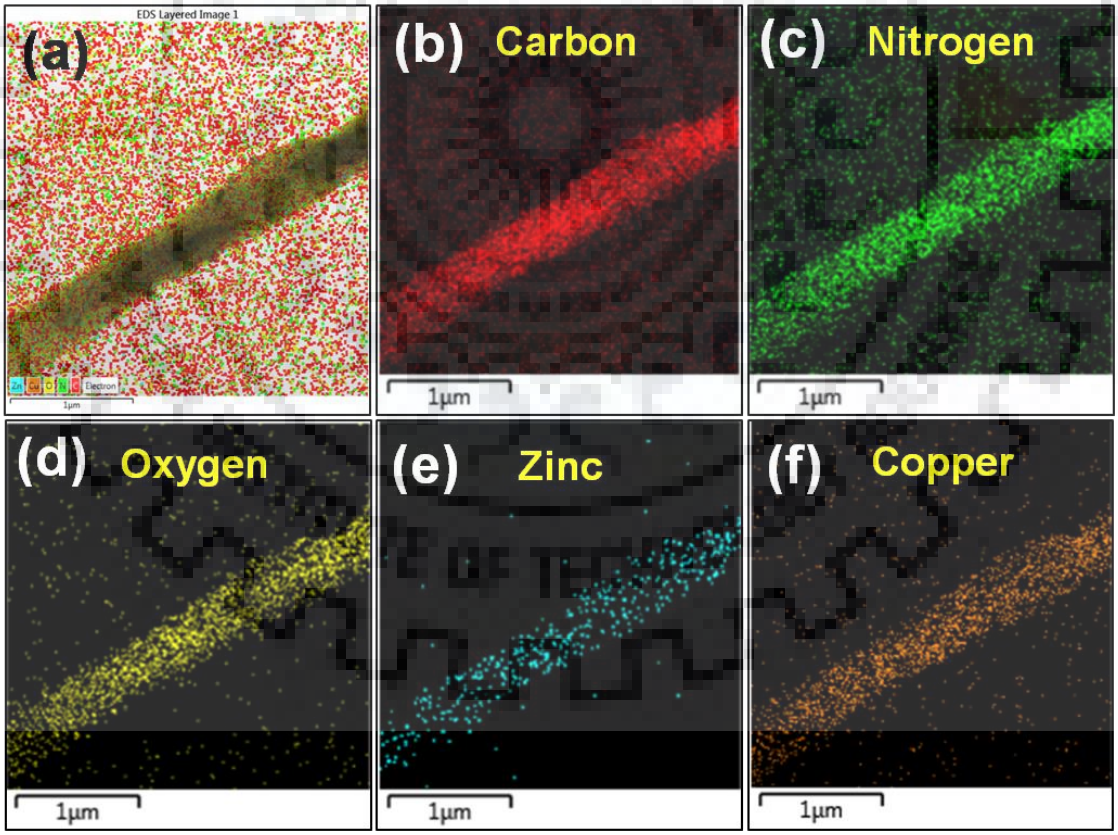

Figure 4.6(a-f) Elemental mapping indicating the uniform distribution of different elements (C, N, O, Zn, Cu)

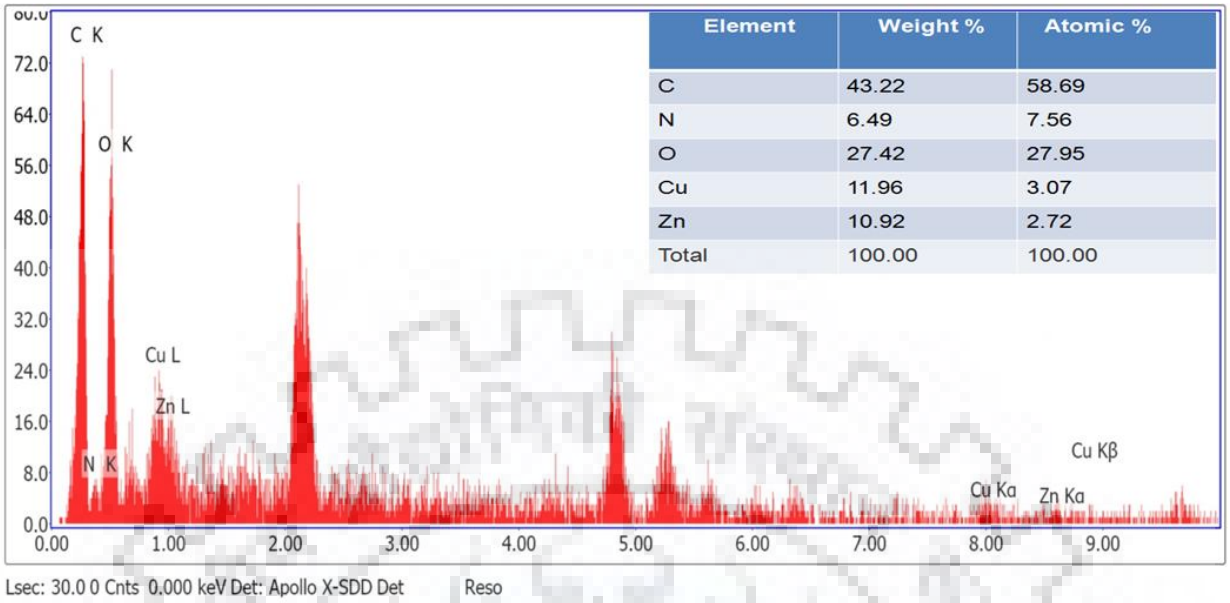

Element	Weight %	Atomic %
C	43.22	58.69
N	6.49	7.56
O	27.42	27.95
Cu	11.96	3.07
Zn	10.92	2.72
Total	100.00	100.00

Figure 4.7 EDX spectra and elemental composition

4.5.2 TEM analysis of calcined sample

Figure 4.8(a-b) represents the TEM images of calcined sample at different magnifications confirming the diameter in the range 130 – 160 nm. Along this SAED pattern (inset in figure 4.8(c)) depicts the polycrystalline nature of the nanofibers as rings are clearly visible. Figure 4.9(a-f) show elemental mapping which illustrates the presence of elements like carbon, oxygen, nitrogen, copper and zinc on nanofiber. Figure 4.10 tells EDX analysis of calcined sample which unfolded the presence of copper (32.65 Wt %) and zinc (30.71 Wt %) on the surface of nanofiber as compared to hydrothermal sample.

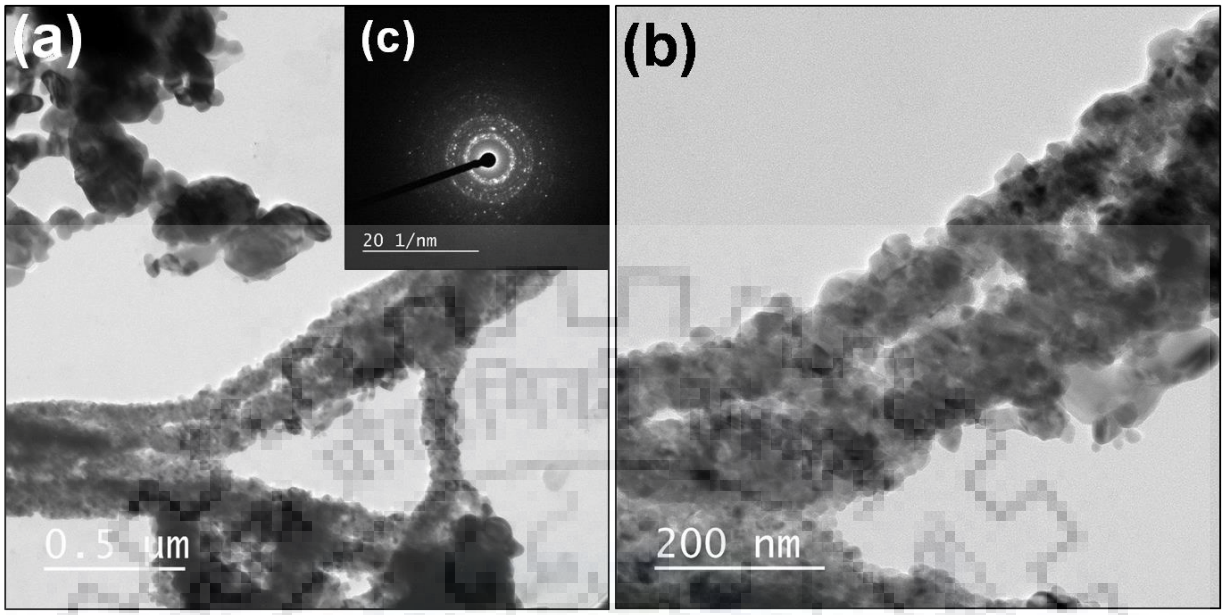

Figure 4.8(a-b) TEM images of calcined sample, (c) its SAED pattern

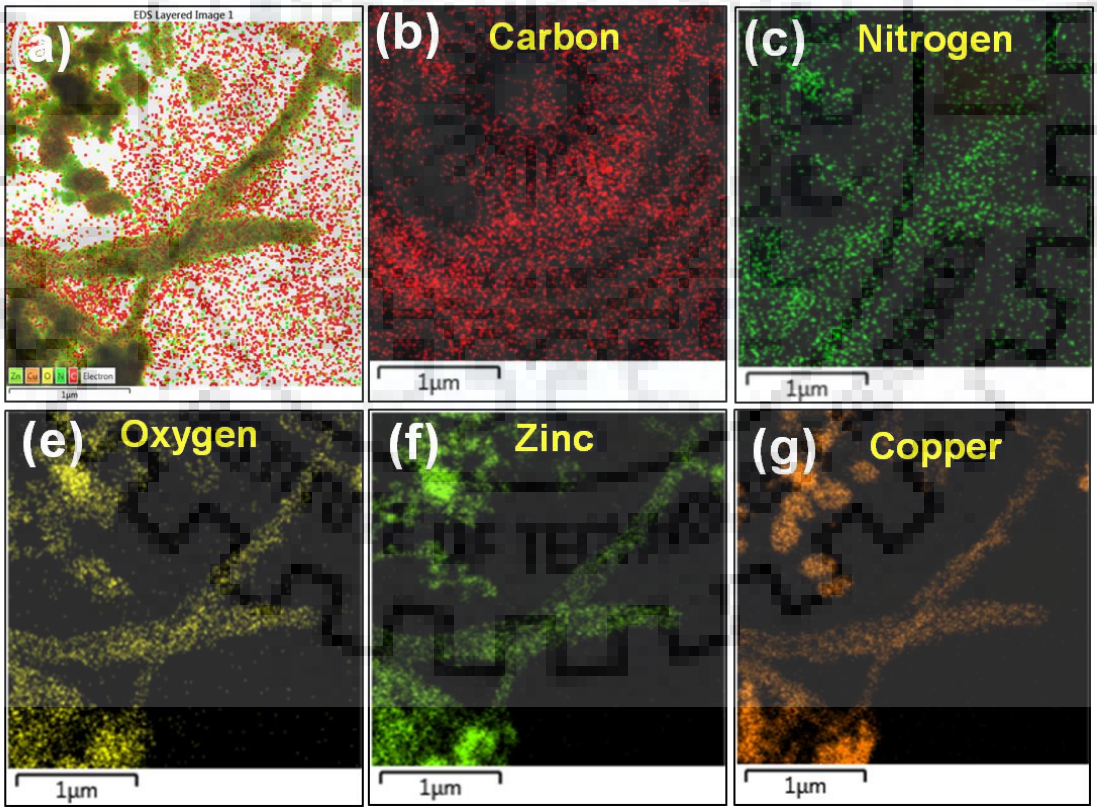

Figure 4.9(a-g) Elemental mapping indicating the uniform distribution of different elements (C, N, O, Zn, Cu)

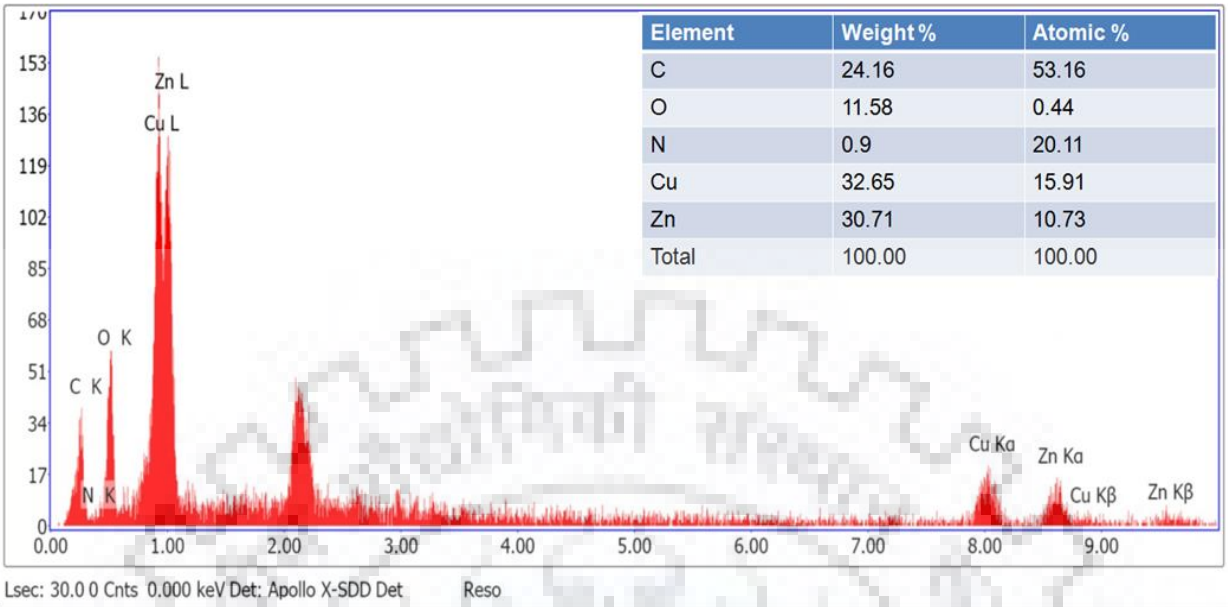

Figure 4.10 EDX spectra and elemental composition

4.6 Diffuse reflectance spectroscopy (DRS) analysis

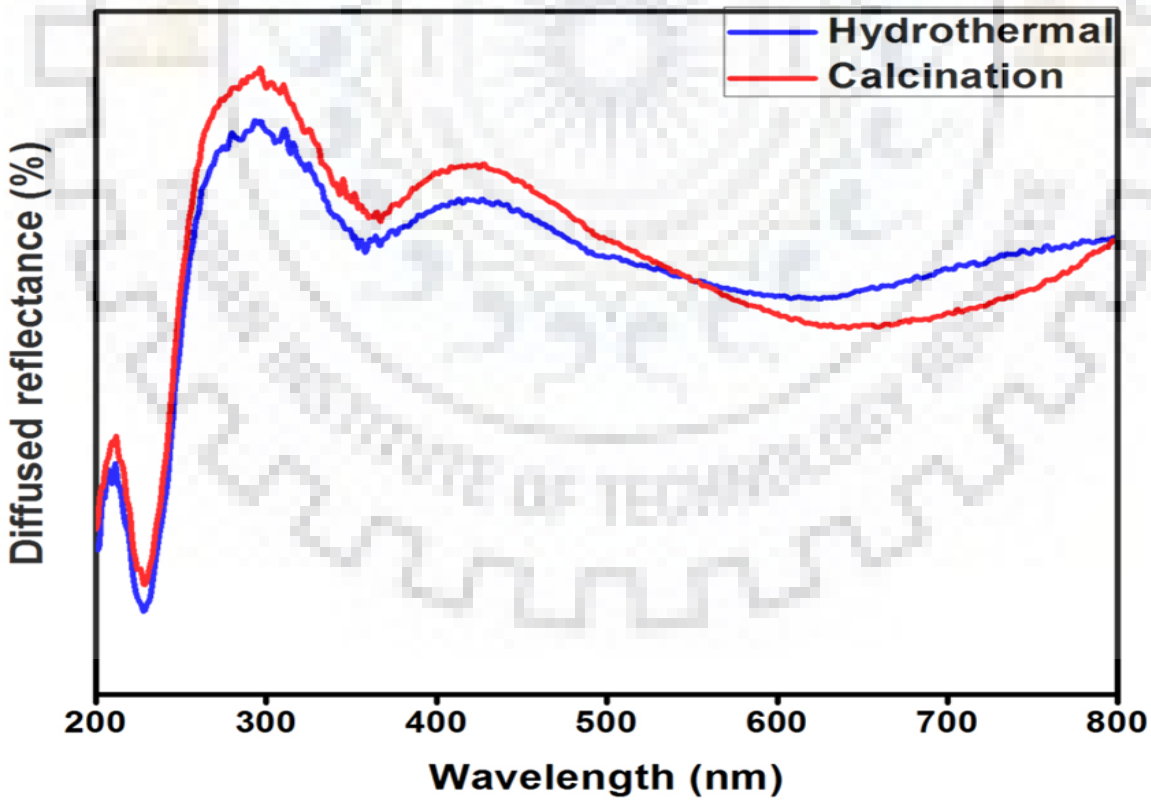

Figure 4.11 UV-VIS-NIR diffuse reflectance specta for both of the samples

The optical properties of synthesized photocatalysts are paramount for photocatalytic applications. The bad gap values of photocatalysts were determined using UV-vis diffuse reflectance spectra (DRS) as illustrated in figure 4.11. To do this, the Kubelka-Munk (K-M) theory was used, which is based on the following equation

$$F(R) = (1- R)^2/ 2R$$

Where, F(R) is Kubelka-Munk (K-M) function and R is absolute reflectance. The band gap energy of photocatalysts can now be evaluated using Kubelka-Munk (K-M) function (F(R)).

$$F(R) \times h\nu = A(h\nu - Eg)^n$$

Where, hv, Eg and A represent energy, band gap energy in eV and proportionality constant respectively. In addition to, n denotes the mode of electronic transition in the semiconductor i.e. n = ½, for direct shift of electron and n = 2, for indirect shift.

From the plots of $[F(R) \times h\nu]^{1/2}$ Vs hν, the band gap values have been calculated. The estimated band gap is 1.56 eV for both of the photocatalysts. Thus, it clearly reveals the formation of p-n heterojunction between CuO and ZnO.

4.7 X-Ray photoelectron spectroscopy (XPS) analysis

XPS measurements were conducted in order to study the electronic states, valencies and chemical oxidation states of the different elements of both samples.

4.7.1 XPS analysis of hydrothermally treated sample

Figure 4.12(a) represents the full spectum of hydrothermally treated sample showing various peaks in the range of 0 to 1200 eV followed by the series of spectra (figure 4.12(b-e)) attributed to the de-convoluted individual spectra of several elements such as C, N, O and Zn respectively. The XPS spectrum (figure 4.12(a)) reveals that C, O, N, Cu & Zn are observed in CuO-ZnO nanofibrous composites and their corresponding photoelectron peaks appeared in binding energies of 284.16 eV (C_{1s}), 399.03 eV (N_{1s}), 531.03 eV (O_{1s}) and 932.2 eV (Cu $_{2p3/2}$). Carbon is homogeneously distributed over the fiber. The N_{1s} signal (figure 4.13(c)) at 399.03 eV is due to polyacrylonitrile (PAN) polymer present in the sample. The oxygen spectra give two signals at

530.86 eV which indicates the formation of metal oxide after hydrothermal treatment and at higher binding energy 531.86 eV corresponds to the O^{-2} of carbonyl group present in metal precursor salts. Figure 4.13(e) shows the core level spectrum of Cu_{2p} which splits into two photoelectron peaks, $Cu_{2p3/2}$ (932.2 eV) and $Cu_{2p3/2}$ (933.6 eV). These binding energies reveal that the oxidation state of copper is +2.

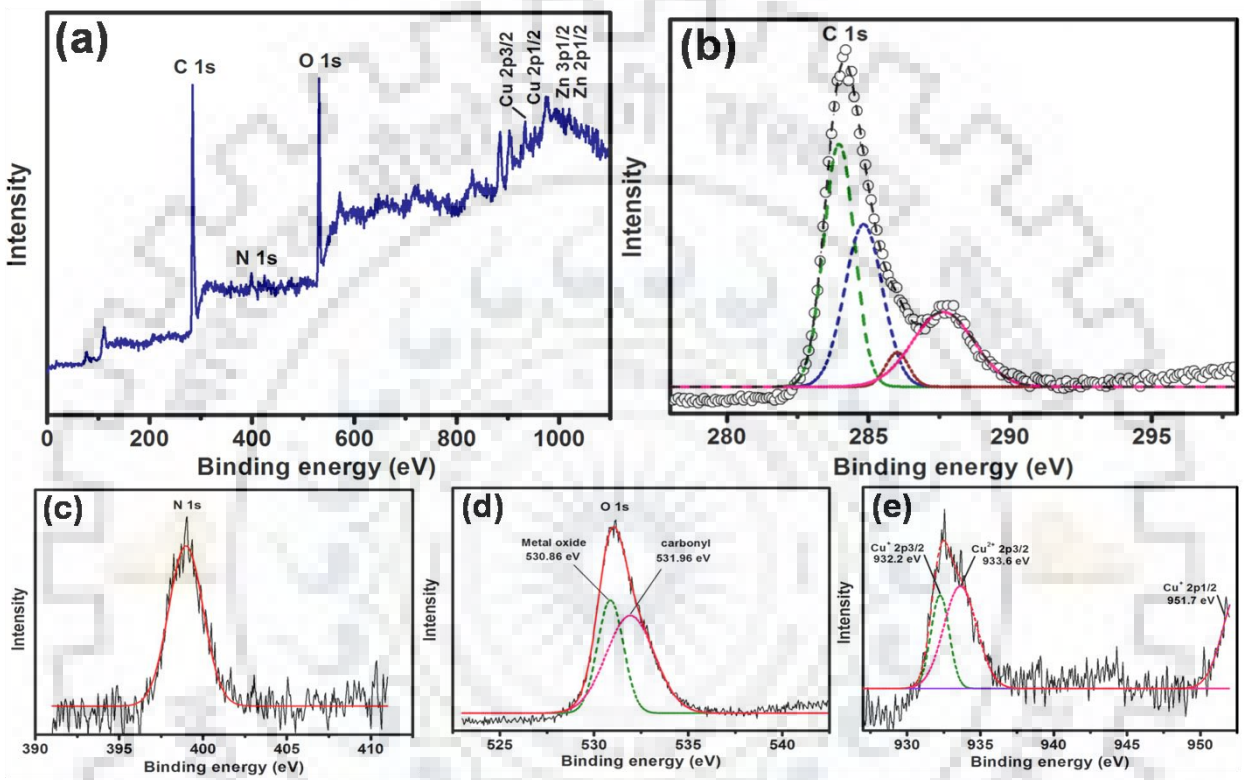

Figure 4.12(a) Full spectrum, (b-e) XPS spectra of C, N, O, Cu of hydrothermal sample

Table 4.2 XPS analysis of different elements found in hydrothermally treated nanofibrous composites and their binding energy values

S. No.	Elements	Binding energy (eV)
1	C_{1s}	284.16
2	N_{1s}	399.03
3	O_{1s}	531.03
4	$Cu^{+}{}_{2p3/2}$ $Cu^{2+}{}_{2p3/2}$	932.20 933.60

4.7.2 XPS analysis of calcined sample

The full spectrum (figure 4.13(a)) indicates the presence of C, N, O, Zn and Cu elements in the calcined nanofibrous composites. In figure 4.13(b), the characteristic peak of C_{1s} found at binding energy 284.53 eV is ascribed to C-C, C-H and C=C bonds. The O_{1s} signal (figure 4.13(c)) is resolved into two components: 529.72 and 531.23 eV which is related to oxidation states of O^{-2} of metal oxide and metal precursor salts. The peak found at 1021.15 eV of $Zn_{3p1/2}$ (figure 4.13(d)) signifies that the formation of ZnO crystal. Peaks centered at binding energies 932.7 and 934.4 eV (figure 4.13(e)) can be attributed to $Cu^{+}{}_{2p3/2}$ and $Cu^{2+}{}_{2p3/2}$ corresponding to the oxidation states of +1 for Cu_2O (Cuprous oxide) and +2 for CuO (Cupric oxide) confirms that two types of metal oxides formed. The difference in the binding energies of oxygen and metals can be due to the influence of different metal oxides formed in the nanofibrous composites.

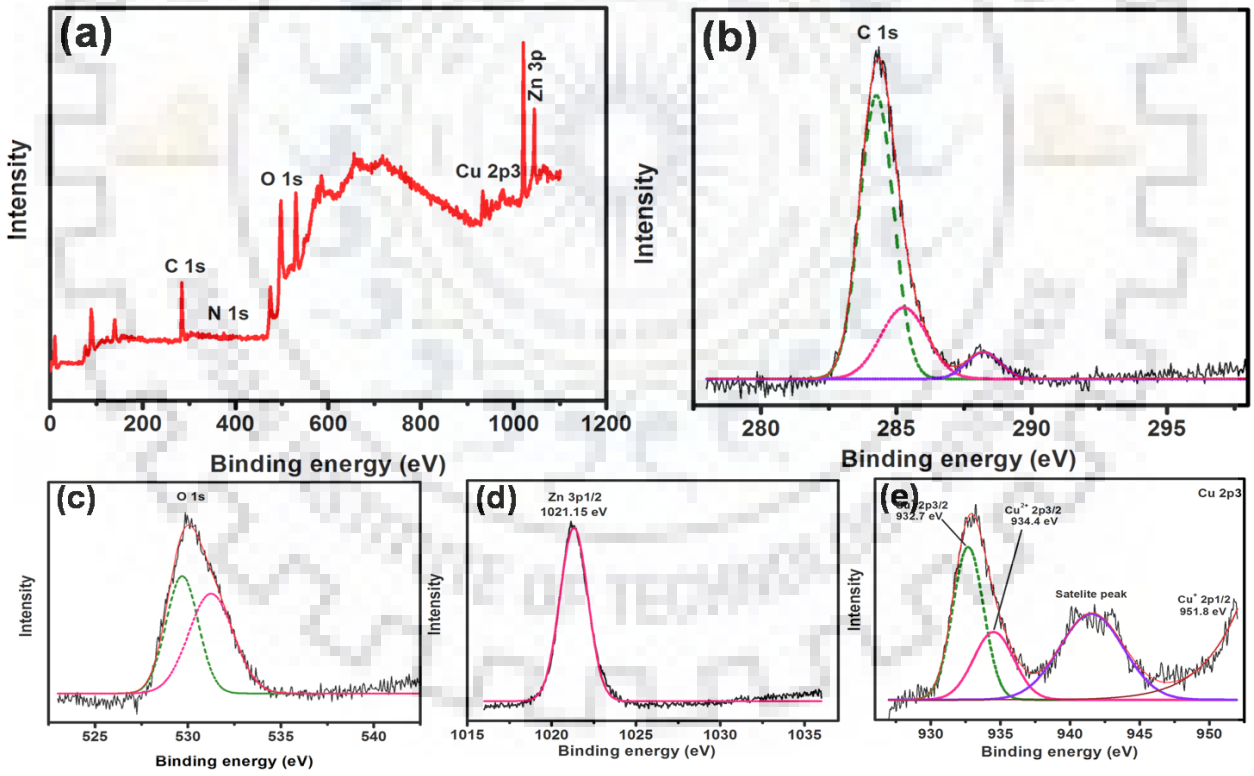

Figure 4.13(a) Full spectrum, (b-e) XPS spectra of C, O, Zn, Cu of calcined sample

Table 4.3 XPS analysis of different elements found in calcined nanofibrous composites and their binding energy values

S. No.	Elements	Binding energy (eV)
1	C_{1s}	284.16
2	O_{1s}	529.97
3	$Zn\ _{3p1/2}$	1021.15
4	$Cu^{+}{}_{2p3/2}$ $Cu^{2+}{}_{2p3/2}$	932.70 934.40

4.8 Photocatalytic studies

Comparative analysis of hydrothermally treated sample and calcined sample

To investigate the better photocatalyst, the efficiencies of both samples were compared.

4.8.1 Control study

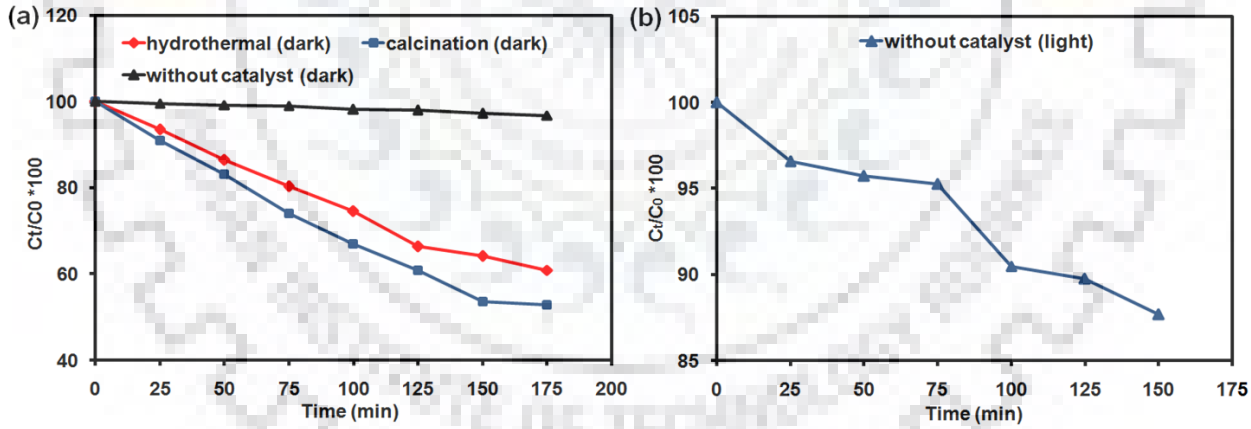

Figure 4.14 Degradation profiles of CR dye (a) with/without catalyst under dark condition, (b) without catalyst under sun light

The photocatalytic activity of the samples was examined by the degradation of CR dye in the presence of sunlight. Before estimating and comparing the photocatalytic activities, some control experiments were performed under different conditions: (a) with/without catalyst under dark conditions and (b) in the presence of sunlight but without catalyst. From figure 4.14(a), it is clearly observed that without any photocatalyst there is very minute reduction in the dye and in

the presence of catalyst, dye is degraded but it takes prodigious amount of time in dark condition. From figure 4.14(b), there is no appreciable degradation of dye without any photocatalyst even in the presence of sunlight. So it indicates equal importance of sunlight as well as catalyst during photocatalytic degradation at the same time.

4.8.2 Time dependent study

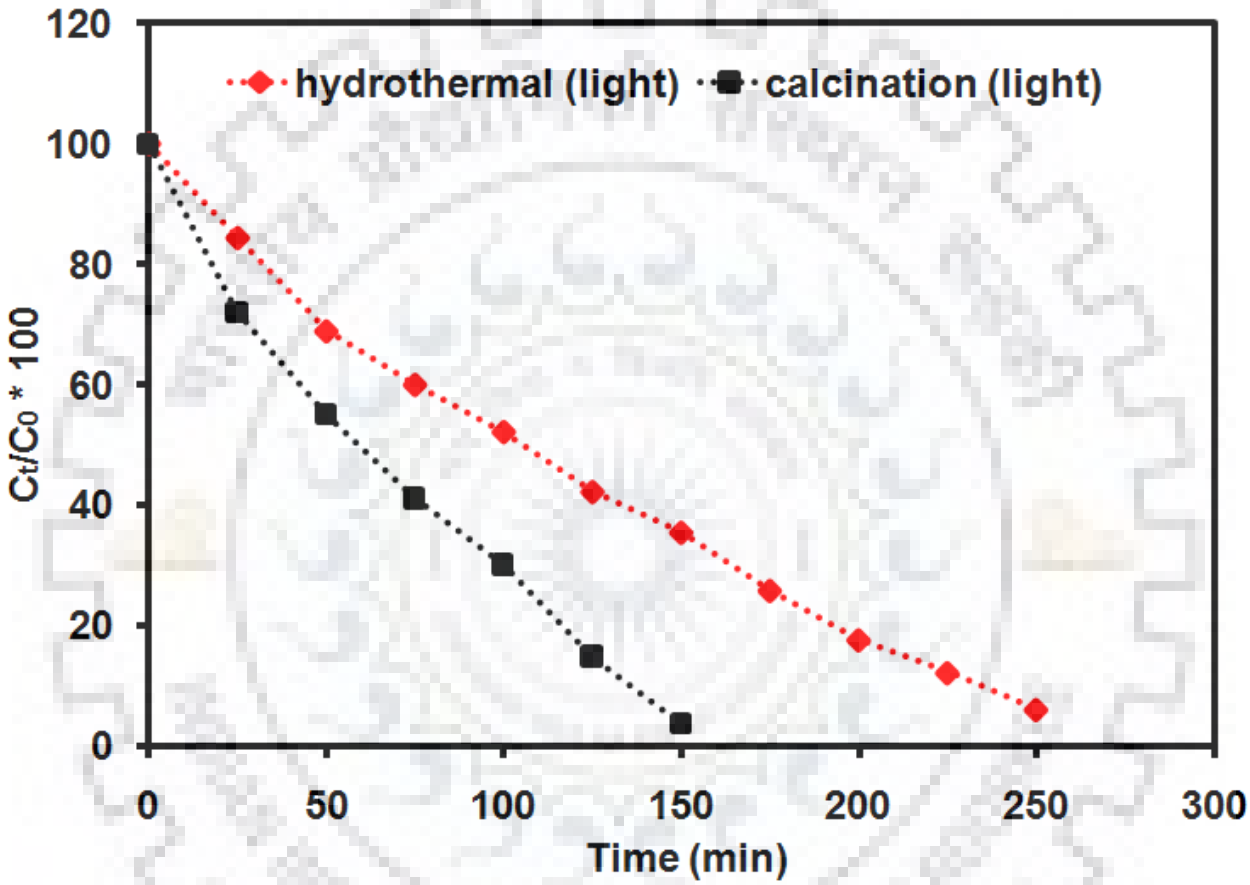

Figure 4.15 Degradation profiles of CR dye in the presence of sunlight

Time dependent study was performed to evaluate the efficiency of the photocatalyst. From figure 4.15, it shows that calcined sample is more efficient with respect to hydrothermally treated sample as it produces more number of hydroxyl free radicals with respect to hydrothermally treated sample within the given interval of time. Moreover, calcined sample (in powder form) has more surface area as compared to hydrothermally treated sample (in leaflet form), so more active sites are available to break azo bonds and naphthalene rings to completely degrade the CR dye.

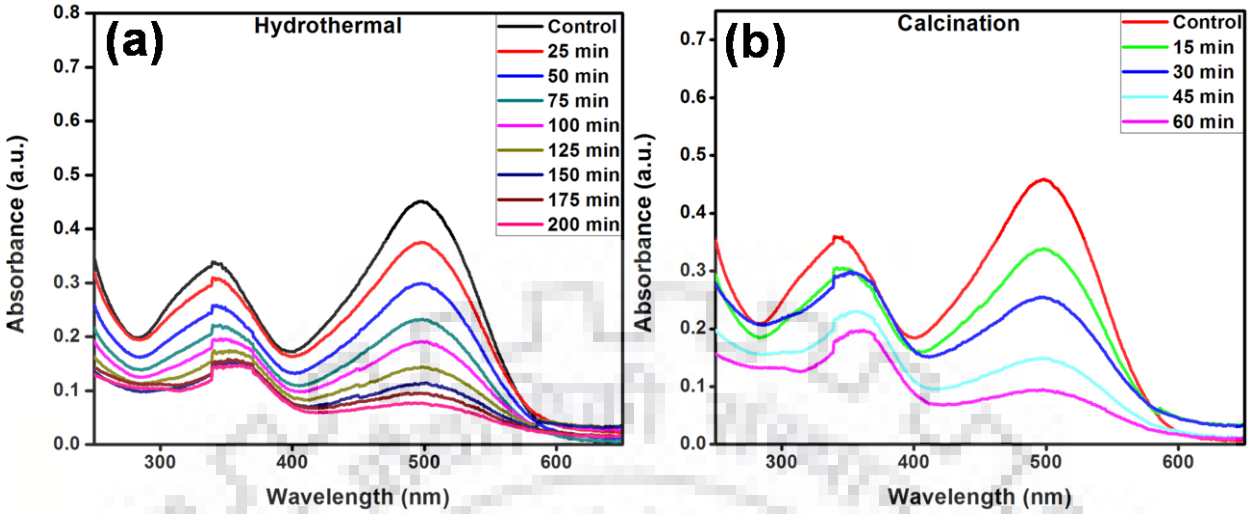

Figure 4.16 UV-Vis spectra of CR dye degradation using (a) hydrothermally treated sample, (b) calcined sample

Figure 4.16(a) and (b) represent UV-Vis spectra for CR dye degradation using hydrothermally treated sample and calcined sample respectively. Same amount of both samples were loaded in the same concentration of dye under similar experimental conditions and absorbance at 500 nm was taken at constant time intervals. It was observed that calcined sample is degrading CR dye faster under solar radiation as compared to hydrothermally treated sample which supports our experimental results.

4.8.3 Kinetic study

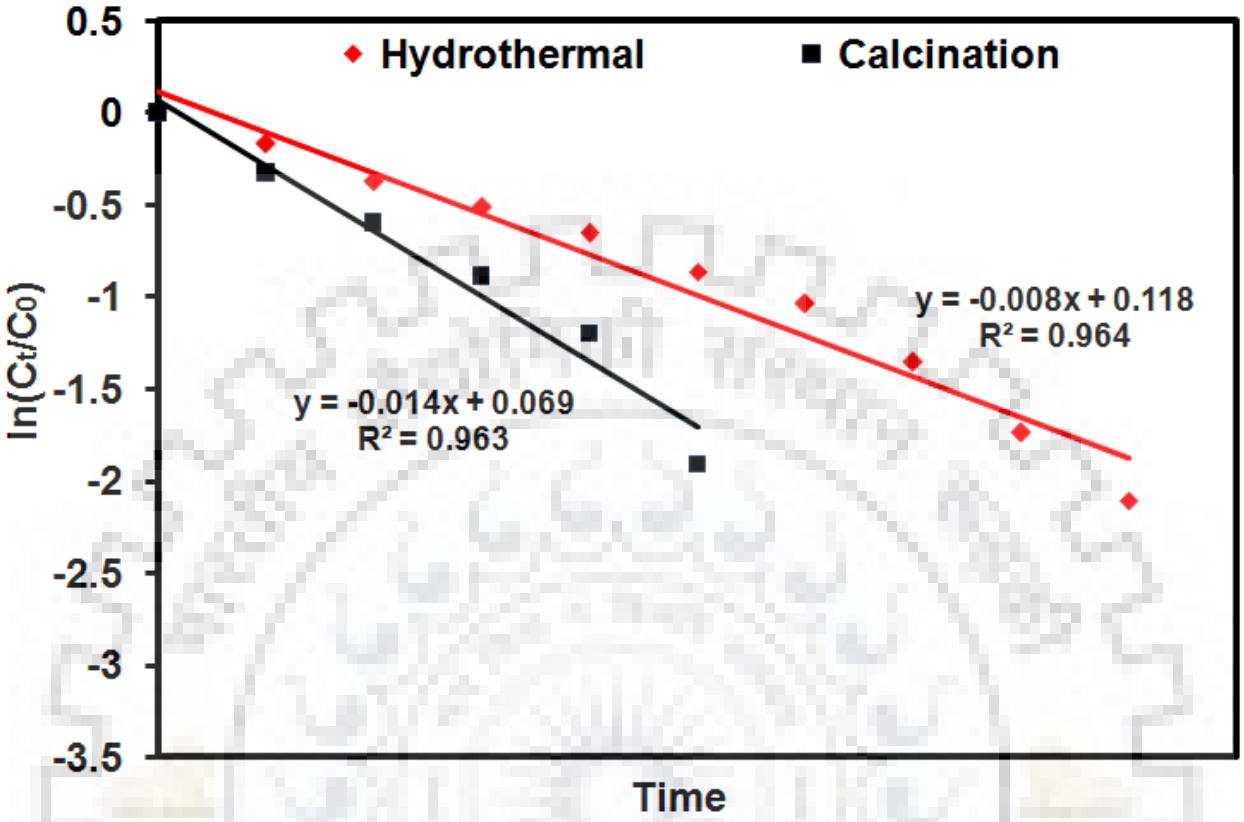

Figure 4.17 represents kinetic study performed with both samples to evaluate rate of degradation

Kinetic study was performed to validate the experimental data of time dependent study as well as to estimate first order rate constant of photocatalytic reaction. The order of reaction was determined by plotting the graph between $\ln(C_0/C_t)$ and time (min) where C_0 is the initial concentration of dye solution and C_t is the concentration of dye at time t. The rate constants for the reactions were calculated from the negative slope of line plotted between $\ln(C_0/C_t)$ Vs time and represented in tabular form (Table 4.4)

Table 4.4 Degradation rate constants calculated for both of the samples

S. No.	Sample	Rate constant (*k*), per minute
1.	Hydrothermally treated	0.8×10^{-2}
2.	Calcined	1.4×10^{-2}

4.8.4 Concentration dependent studies

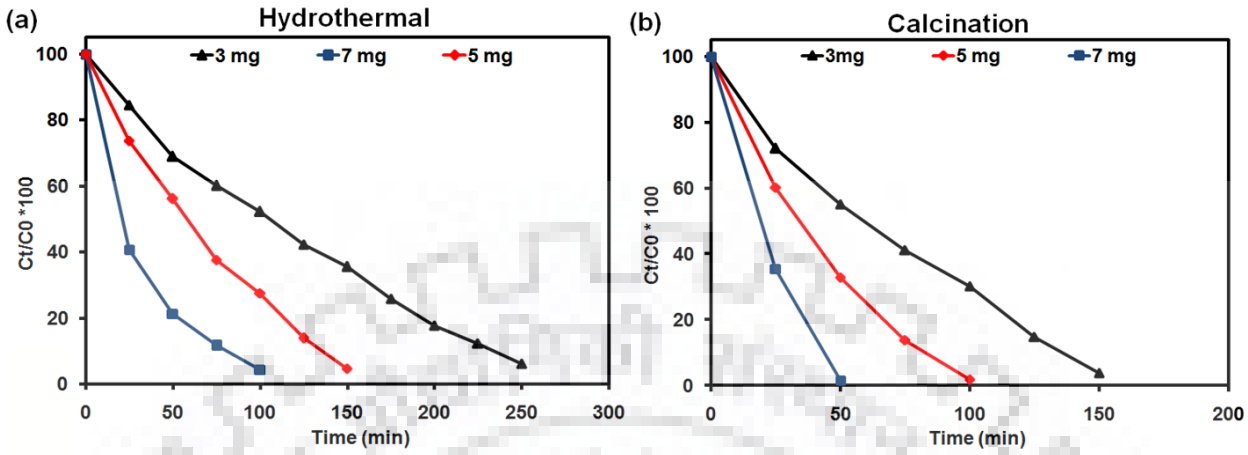

Figure 4.18 (a, b) representing concentration dependent studies performed with both samples using same concentration of dye (180 ppm)

The amount of photocatalyst to be added plays a significant role in dye degradation. As the molar mass of catalyst added increases, the rate of dye degradation will be faster and time of degradation declines as more surface area will be available as well as more number of free radicals will be generated to degrade the same amount dye present in fresh dye solution. From figure 4.18(a), it was observed that within 100 min, 180 ug/mL concentration of dye was totally degraded with 7 mg of catalyst (hydrothermally treated) while it took 150 and 250 min for 5 mg and 3 mg of catalyst respectively. From Figure 4.18(b), 7 mg of photocatalyst (calcined) took less time to completely degrade CR dye solution with respect to 3 mg and 5 mg of same catalyst under same experimental conditions. Degradation rate constants were calculated for both of the samples and tabulated in table 4.5 and 4.6.

Table 4.5 Rate constants calculated for different concentrations of hydrothermally treated sample

S. No.	Amount of catalyst loaded (hydrothermally treated)	Rate constant (*k*), per minute
1.	3 mg	3.62×10^{-1}
2.	5 mg	6.20×10^{-1}
3.	7 mg	8.81×10^{-1}

Table 4.6 Rate constants calculated for different concentrations of calcined sample

S. No.	Amount of catalyst loaded (calcined)	Rate constant (*k*), per minute
1.	3 mg	6.11×10^{-1}
2.	5 mg	9.70×10^{-1}
3.	7 mg	19.67×10^{-1}

4.9 Photoluminescence (PL) studies

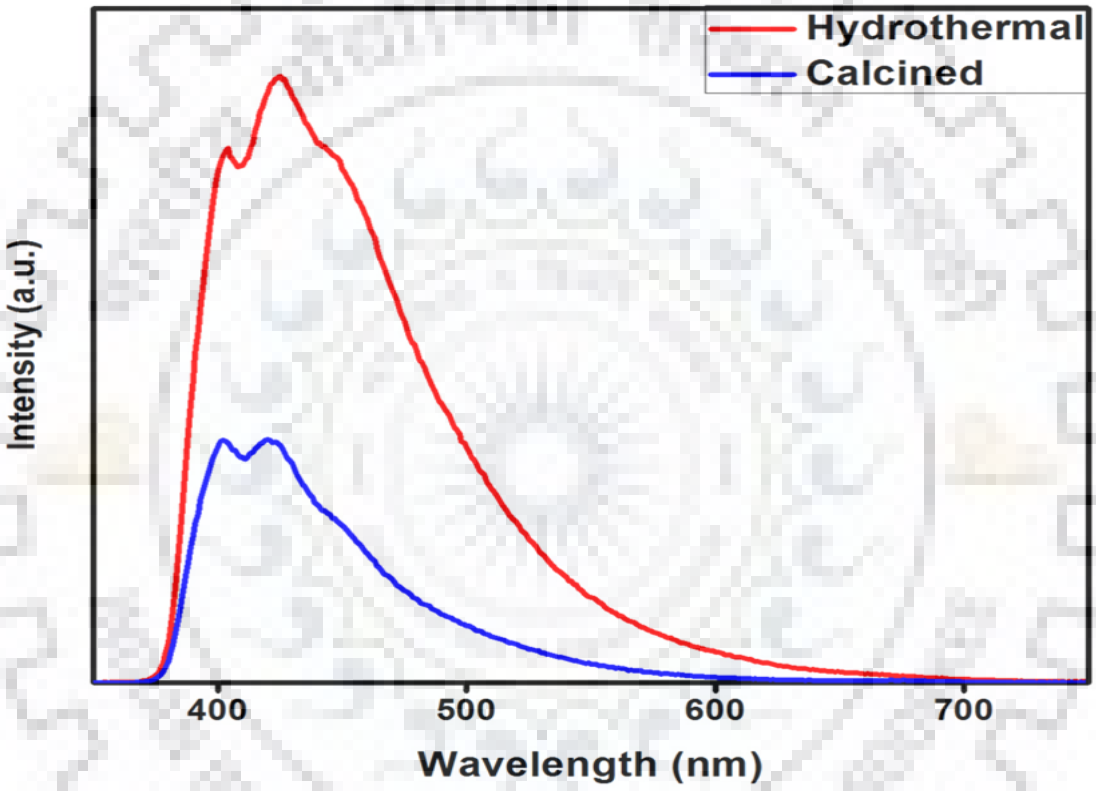

Figure 4.19 Photoluminescence (PL) emission spectra for both of the samples

To further investigate recombination/separation rate of charge carriers, photoluminescence studies (PL) were performed. From the above figure 4.19, it was observed that PL intensity of calcined sample was lower than that of hydrothermally treated sample which showed the better charge separation, lower recombination rate and better photocatalytic activity in case of calcined sample as compared to later. The hydrothermally treated sample exhibited a visible emission peak centered at around 425 nm^{-1} and for calcined sample, PL signal with peak maximum at 410 nm^{-1}. Thus, this analysis reveals that calcined sample has more photocatalytic activity which supports our kinetic study.

4.10 Reusability studies

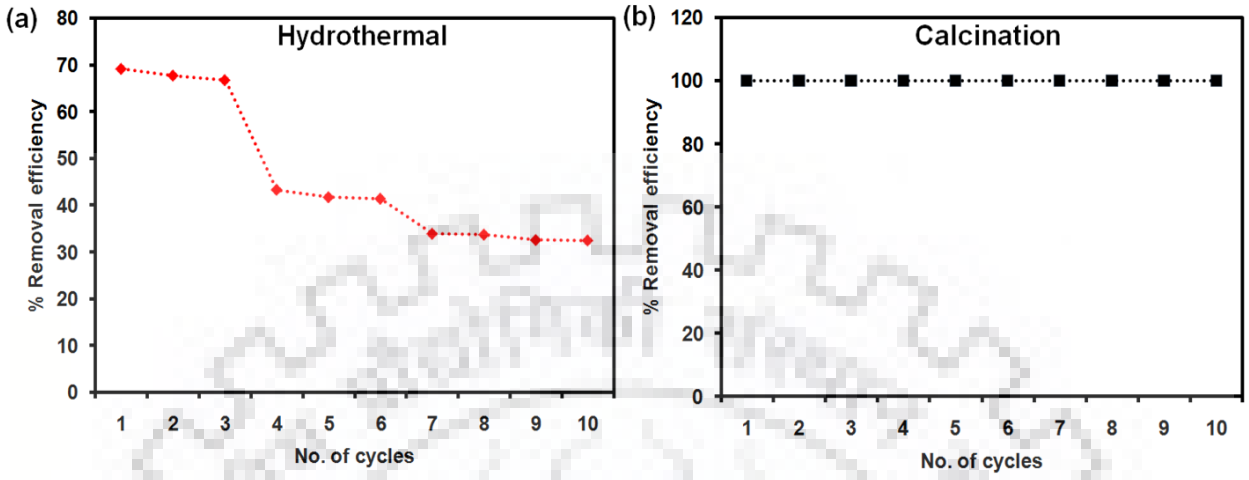

Figure 4.20 (a, b) Reusability studies performed with both samples up to ten cycles under same experimental conditions

The reusability study of both samples was performed to evaluate viability of multiple utilizations in the degradation of organic dyes. In photocatalytic applications the stability of photocatalyst is extremely important as it can abate the overall cost of the dye in multiple times in waste water treatment. To this end, ten successive cycles of photocatalytic dye degradation were performed utilizing both samples with fresh dye solution. The results of cycling experiments carried out by both samples are represented in figure 4.20(a) and (b), respectively. Figure 4.20(a) indicates that after three consecutive cycles, the photocatalytic activity of hydrothermally treated sample decreases and retains its stability for next three successive cycles and further declines for the rest of the cycles. However, the calcined sample exhibited excellent photocatalytic activity subsequently for all the cycles. In addition to this, the structural integrity of photocatalyst is also preserved even after ten cycles reflecting the high stability of the materials. From the resusability experiment, the practical applicability of calcined and hydrothermally treated composite materials can be effectively utilized for the sunlight mediated photocatalytic dye degradation application.

CHAPTER 5
CONCLUDING REMARKS

5.1 Conclusion

In summary, we have successfully fabricated CuO-ZnO nanofibrous composites using simple electrospinning technique followed by post heat treatment methods i.e. hydrothermal and calcination. The synthesized nanofibrous materials were characterized by several analytical techniqiues. The comprehensive batch wise dye degradation and kinetic studies supplemented the effective photocatalytic activity of the synthesized nanomaterials. It was observed that CuO-ZnO nanofibrous composites degrade organic CR dye into less toxic CO_2 and water by the solar irradiation. From the experimental results it was ascertained that the calcined sample showed higher degradation rate towards CR dye due to the higher separation rate of charge carriers as well as large surface area with respect to the hydrothermally treated sample. Moreover, concentration of photocatalyst plays a significant role in dye degradation in which more amount of catalyst, faster is the degradation rate. In addition to this, stability and reusability are additional advantages of these materials. The calcined sample exhibited 100 % degradation consecutively for ten cycles whereas, in the case of hydrothermal treated sample degradation efficiency gradually decreases in the subsequent cycles. Therefore, calcined sample stands out as appropriate candidate for application in the large scale industrial waste water treatment plants.

5.2 Future scope of the work

After comprehensive analysis and experiments, a laboratory based photocatalytic reactor needs to be developed in which the synthetic polymeric nanofibrous sheet to be placed at the bottom of the reactor and the toxic dye pollutants undergo degradation through photocatalysis under solar irradiation followed by collection of treated water through the outlets and the same idea can be scaled up as per industrial requirements.

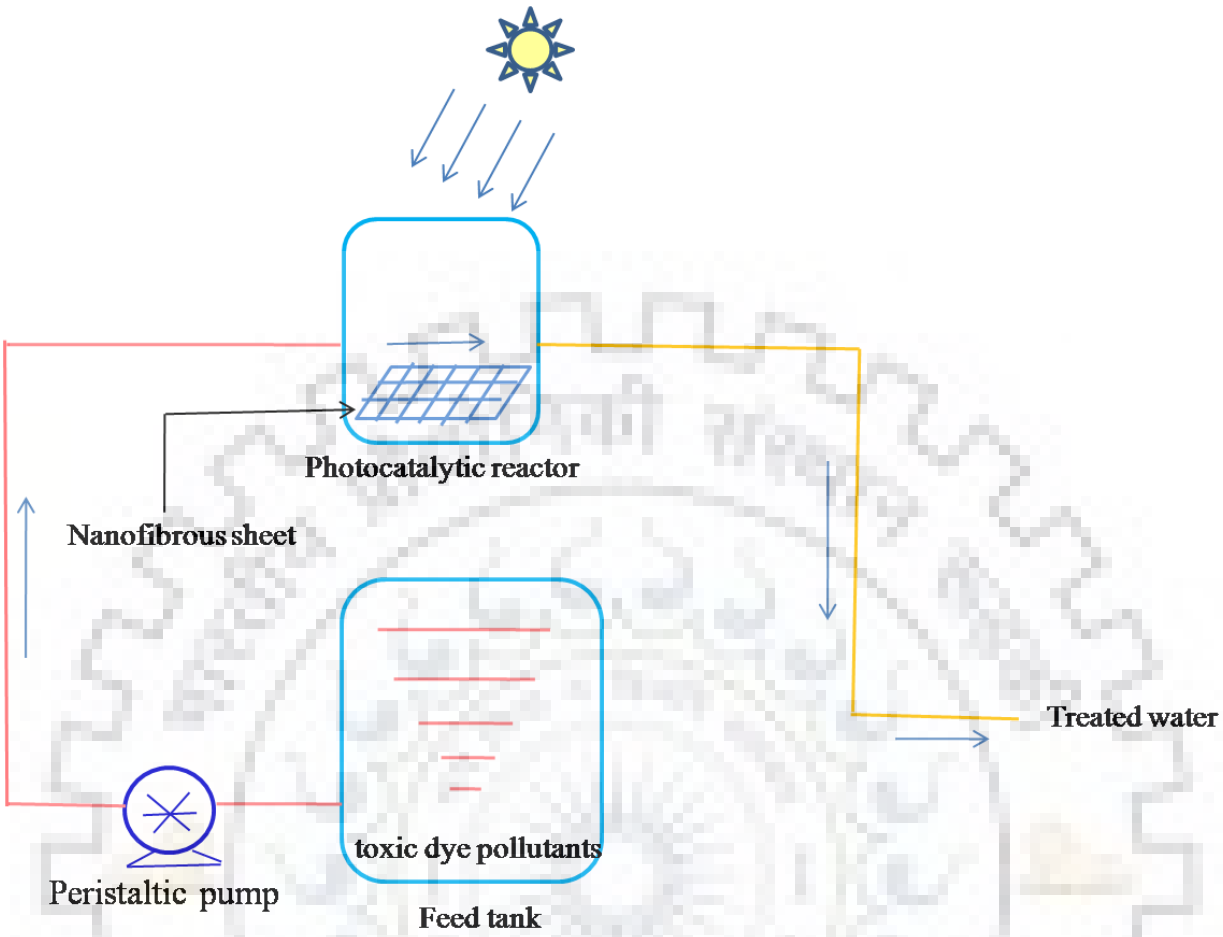

Figure 5.1 Proposed laboratory photocatalytic reactor

CHAPTER 6
REFERENCES

REFERENCES

(1) Puvaneswari, N.; Muthukrishnan, J.; Gunasekaran, P. Toxicity Assessment and Microbial Degradation of Azo Dyes. *Indian Journal of Experimental Biology*. 2006, pp 618–626.

(2) Malwal, D.; Gopinath, P. Efficient Adsorption and Antibacterial Properties of Electrospun CuO-ZnO Composite Nanofibers for Water Remediation. *J. Hazard. Mater.* **2017**, *321*, 611–621.

(3) Liu, L.; Gao, Z. Y.; Su, X. P.; Chen, X.; Jiang, L.; Yao, J. M. Adsorption Removal of Dyes from Single and Binary Solutions Using a Cellulose-Based Bioadsorbent. *ACS Sustain. Chem. Eng.* **2015**, *3* (3), 432–442.

(4) Razak, M. R.; Yusof, N. A.; Haron, M. J.; Ibrahim, N.; Mohammad, F.; Kamaruzaman, S.; Al-Lohedan, H. A. Iminodiacetic Acid Modified Kenaf Fiber for Waste Water Treatment. *Int. J. Biol. Macromol.* **2018**, *112*, 754–760.

(5) Garg, V. K.; Kumar, R.; Gupta, R. Removal of Malachite Green Dye from Aqueous Solution by Adsorption Using Agro-Industry Waste: A Case Study of Prosopis Cineraria. *Dye. Pigment.* **2004**, *62* (1), 1–10.

(6) Rinde, E.; Troll, W. Metabolic Reduction of Benzidine Azo Dyes to Benzidine in the Rhesus Monkey. *J Natl Cancer Inst* **1975**, *55* (1), 181–2.

(7) Zollinger, H. *Color Chemistry: Syntheses, Properties, and Applications of Organic Dyes and Pigments*; 1991; Vol. 11.

(8) Tiwari, D. K.; Behari, J.; Sen, P. Application of Nanoparticles in Waste Water Treatment. *Carbon Nanotub.* **2008**, *3* (3), 417–433.

(9) Rincón, A. G.; Pulgarin, C. Use of Coaxial Photocatalytic Reactor (CAPHORE) in the TiO2 Photo-Assisted Treatment of Mixed E. Coli and Bacillus Sp. and Bacterial

Community Present in Wastewater. In *Catalysis Today*; 2005; Vol. 101, pp 331–344.

(10) Park, K. Y.; Choi, S. Y.; Lee, S. H.; Kweon, J. H.; Song, J. H. Comparison of Formation of Disinfection by-Products by Chlorination and Ozonation of Wastewater Effluents and Their Toxicity to Daphnia Magna. *Environ. Pollut.* **2016**, *215*, 314–321.

(11) Choksumlitpol, P.; Mangkornkarn, C.; Sumtong, P.; Onlaor, K.; Eiad-Ua, A. Fabrication of Anodic Titanium Oxide (ATO) for Waste Water Treatment Application. In *Materials Today: Proceedings*; 2017; Vol. 4, pp 6124–6128.

(12) Zhu, H.; Jiang, R.; Xiao, L.; Chang, Y.; Guan, Y.; Li, X.; Zeng, G. Photocatalytic Decolorization and Degradation of Congo Red on Innovative Crosslinked Chitosan/nano-CdS Composite Catalyst under Visible Light Irradiation. *J. Hazard. Mater.* **2009**, *169* (1–3), 933–940.

(13) Konstantinou, I. K.; Albanis, T. A. TiO2-Assisted Photocatalytic Degradation of Azo Dyes in Aqueous Solution: Kinetic and Mechanistic Investigations: A Review. *Appl. Catal. B Environ.* **2004**, *49* (1), 1–14.

(14) Sadollahkhani, A.; Hussain Ibupoto, Z.; Elhag, S.; Nur, O.; Willander, M. Photocatalytic Properties of Different Morphologies of CuO for the Degradation of Congo Red Organic Dye. *Ceram. Int.* **2014**, *40* (7 PART B).

(15) Hristovski, K. D.; Westerhoff, P. K.; Crittenden, J. C.; Olson, L. W. Arsenate Removal by Nanostructured ZrO2 Spheres. *Environ. Sci. Technol.* **2008**, *42* (10), 3786–3790.

(16) Jing, L.; Zhou, W.; Tian, G.; Fu, H. Surface Tuning for Oxide-Based Nanomaterials as Efficient Photocatalysts. *Chem. Soc. Rev.* **2013**, *42* (24), 9509.

(17) Xia, Y.; Yang, P.; Sun, Y.; Wu, Y.; Mayers, B.; Gates, B.; Yin, Y.; Kim, F.; Yan, H. One-Dimensional Nanostructures: Synthesis, Characterization, and Applications. *Adv. Mater.* **2003**, *15* (5), 353–389.

(18) Liu, L.; Liu, Z.; Bai, H.; Sun, D. D. Concurrent Filtration and Solar Photocatalytic Disinfection/degradation Using High-Performance Ag/TiO 2 Nanofiber Membrane. *Water Res.* **2012**, *46* (4), 1101–1112.

(19) Feng, C.; Khulbe, K. C.; Matsuura, T.; Tabe, S.; Ismail, A. F. Preparation and Characterization of Electro-Spun Nanofiber Membranes and Their Possible Applications in Water Treatment. *Separation and Purification Technology*. 2013, pp 118–135.

(20) Vamvakaki, V.; Tsagaraki, K.; Chaniotakis, N. Carbon Nanofiber-Based Glucose Biosensor. *Anal. Chem.* **2006**, *78* (15), 5538–5542.

(21) Yoshimoto, H.; Shin, Y. M.; Terai, H.; Vacanti, J. P. A Biodegradable Nanofiber Scaffold by Electrospinning and Its Potential for Bone Tissue Engineering. *Biomaterials* **2003**, *24* (12), 2077–2082.

(22) Hrib, J.; Sirc, J.; Hobzova, R.; Hampejsova, Z.; Bosakova, Z.; Munzarova, M.; Michalek, J. Nanofibers for Drug Delivery - Incorporation and Release of Model Molecules, Influence of Molecular Weight and Polymer Structure. *Beilstein J. Nanotechnol.* **2015**, *6* (1), 1939–1945.

(23) Ozin, G. A.; Hou, K.; Lotsch, B. V.; Cademartiri, L.; Puzzo, D. P.; Scotognella, F.; Ghadimi, A.; Thomson, J. Nanofabrication by Self-Assembly. *Materials Today*. 2009, pp 12–23.

(24) Guiton, B. S.; Davies, P. K. Nano-Chessboard Superlattices Formed by Spontaneous Phase Separation in Oxides. *Nat. Mater.* **2007**, *6* (8), 586–591.

(25) Huang, Z. M.; Zhang, Y. Z.; Kotaki, M.; Ramakrishna, S. A Review on Polymer Nanofibers by Electrospinning and Their Applications in Nanocomposites. *Compos. Sci. Technol.* **2003**, *63* (15), 2223–2253.

(26) Grzelczak, M.; Vermant, J.; Furst, E. M.; Liz-Marzán, L. M. Directed Self-Assembly of Nanoparticles. *ACS Nano*. 2010, pp 3591–3605.

(27) Liu, Y.; Chen, X.; Li, J.; Burda, C. Photocatalytic Degradation of Azo Dyes by Nitrogen-Doped TiO2 Nanocatalysts. *Chemosphere* **2005**, *61* (1), 11–18.

(28) Ichimori, T.; Mizuma, K.; Uchida, T.; Yamazaki, S.; Kimura, K. Morphological Diversity and Nanofiber Networks of Poly(p-Oxybenzoyl) Generated by Phase Separation during Copolymerization. *J. Appl. Polym. Sci.* **2013**, *128* (2), 1282–1290.

(29) Huang, L.; McMillan, R. A.; Apkarian, R. P.; Pourdeyhimi, B.; Conticello, V. P.; Chaikof, E. L. Generation of Synthetic Elastin-Mimetic Small Diameter Fibers and Fiber Networks. *Macromolecules* **2000**, *33* (8), 2989–2997.

(30) Pawlowski, K. J.; Barnes, C. P.; Boland, E. D.; Wnek, G. E.; Bowlin, G. L. Biomedical Nanoscience: Electrospinning Basic Concepts, Applications, and Classroom Demonstration. *Mat. Res. Soc. Symp. Proc.* **2004**, *827*, BB1.7.1-BB1.7.12.

(31) Li, D.; Wang, Y.; Xia, Y. Electrospinning Nanofibers as Uniaxially Aligned Arrays and Layer-by-Layer Stacked Films. *Adv. Mater.* **2004**, *16* (4), 361–366.

(32) Xie, J.; Hsieh, Y. Lo. Ultra-High Surface Fibrous Membranes from Electrospinning of Natural Proteins: Casein and Lipase Enzyme. In *Journal of Materials Science*; 2003; Vol. 38, pp 2125–2133.

(33) Kumbar, S. G.; James, R.; Nukavarapu, S. P.; Laurencin, C. T. Electrospun Nanofiber Scaffolds: Engineering Soft Tissues. *Biomed. Mater.* **2008**, *3* (3).

(34) An, S.; Joshi, B. N.; Lee, M. W.; Kim, N. Y.; Yoon, S. S. Electrospun Graphene-ZnO Nanofiber Mats for Photocatalysis Applications. *Appl. Surf. Sci.* **2014**, *294*, 24–28.

(35) Thavasi, V.; Singh, G.; Ramakrishna, S. Electrospun Nanofibers in Energy and Environmental Applications. *Energy Environ. Sci.* **2008**, *1* (2), 205.

(36) Choi, J.; Chan, S.; Joo, H.; Yang, H.; Ko, F. K. Three-Dimensional (3D) Palladium-Zinc Oxide Nanowire Nanofiber as Photo-Catalyst for Water Treatment. *Water Res.* **2016**, *101*, 362–369.

(37) Malwal, D.; Gopinath, P. Fabrication and Applications of Ceramic Nanofibers in Water Remediation: A Review. *Critical Reviews in Environmental Science and Technology*. 2016, pp 500–534.

(38) Thompson, C. J.; Chase, G. G.; Yarin, A. L.; Reneker, D. H. Effects of Parameters on Nanofiber Diameter Determined from Electrospinning Model. *Polymer (Guildf).* **2007**, *48* (23), 6913–6922.

(39) Beachley, V.; Wen, X. Effect of Electrospinning Parameters on the Nanofiber Diameter and Length. *Mater. Sci. Eng. C* **2009**, *29* (3), 663–668.

(40) Tan, Y. N.; Wong, C. L.; Mohamed, A. R. An Overview on the Photocatalytic Activity of Nano-Doped-TiO2 in the Degradation of Organic Pollutants. *ISRN Mater. Sci.* **2011**, *2011*, 1–18.

(41) Khurana, R.; Uversky, V. N.; Nielsen, L.; Fink, A. L. Is Congo Red an Amyloid-Specific Dye? *J. Biol. Chem.* **2001**, *276* (25), 22715–22721.

(42) Thapa, R.; Maiti, S.; Rana, T. H.; Maiti, U. N.; Chattopadhyay, K. K. Anatase TiO2nanoparticles Synthesis via Simple Hydrothermal Route: Degradation of Orange II, Methyl Orange and Rhodamine B. *J. Mol. Catal. A Chem.* **2012**, *363–364*, 223–229.

(43) Zhang, Y.; Chen, Y.; Hou, L.; Guo, F.; Liu, J.; Qiu, S.; Xu, Y.; Wang, N.; Zhao, Y. Pine-Branch-like TiO_2 Nanofibrous Membrane for High Efficiency Strong Corrosive Emulsion Separation. *J. Mater. Chem. A* **2017**, *5* (31), 16134–16138.

(44) Wang, H. W.; Hu, Z. A.; Chang, Y. Q.; Chen, Y. L.; Lei, Z. Q.; Zhang, Z. Y.; Yang, Y. Y. Facile Solvothermal Synthesis of a Graphene Nanosheet-Bismuth Oxide Composite and Its Electrochemical Characteristics. *Electrochim. Acta* **2010**, *55* (28), 8974–8980.

(45) Fan, J.; Li, T.; Heng, H. Hydrothermal Growth of ZnO Nanoflowers and Their Photocatalyst Application. *Bull. Mater. Sci.* **2016**, *39* (1), 19–26.

(46) Kim, S. O.; Shim, J. B.; Chang, H. Rapid Hydrothermal Synthesis of Zinc Oxide Nanowires by Annealing Methods on Seed Layers. *J. Nanomater.* **2011**, *2011*.

(47) Baruah, S.; Dutta, J. Hydrothermal Growth of ZnO Nanostructures. *Sci. Technol. Adv. Mater.* **2009**, *10* (1), 13001.

(48) Yang, L. Y.; Dong, S. Y.; Sun, J. H.; Feng, J. L.; Wu, Q. H.; Sun, S. P. Microwave-Assisted Preparation, Characterization and Photocatalytic Properties of a Dumbbell-Shaped ZnO Photocatalyst. *J. Hazard. Mater.* **2010**, *179* (1–3), 438–443.

(49) He, L.; Tong, Z.; Wang, Z.; Chen, M.; Huang, N.; Zhang, W. Effects of Calcination

Temperature and Heating Rate on the Photocatalytic Properties of ZnO Prepared by Pyrolysis. *J. Colloid Interface Sci.* **2018**, *509*, 448–456.

(50) Taheri Mofassal, A.; Tajally, M.; Mirzaee, O. Comparison between Microwave and Conventional Calcination Techniques in Regard to Reactivity and Morphology of Co-Precipitated BaTiO3powder, and the Electrical and Energy Storage Properties of the Sintered Samples. *Ceram. Int.* **2017**, *43* (11), 8057–8064.

(51) Salavati-Niasari, M.; Davar, F. Synthesis of Copper and copper(I) Oxide Nanoparticles by Thermal Decomposition of a New Precursor. *Mater. Lett.* **2009**, *63* (3–4), 441–443.

(52) Betancourt-Galindo, R.; Reyes-Rodriguez, P. Y.; Puente-Urbina, B. A.; Avila-Orta, C. A.; Rodríguez-Fernández, O. S.; Cadenas-Pliego, G.; Lira-Saldivar, R. H.; García-Cerda, L. A. Synthesis of Copper Nanoparticles by Thermal Decomposition and Their Antimicrobial Properties. *J. Nanomater.* **2014**, *2014*.

(53) Pawar, R. C.; Cho, D.; Lee, C. S. Fabrication of Nanocomposite Photocatalysts from Zinc Oxide Nanostructures and Reduced Graphene Oxide. *Curr. Appl. Phys.* **2013**, *13* (4 SUPPL.2).

(54) Khan, M. M.; Adil, S. F.; Al-Mayouf, A. Metal Oxides as Photocatalysts. *Journal of Saudi Chemical Society*. 2015, pp 462–464.

(55) Uddin, M. T. Metal Oxide Heterostructures for Efficient Photocatalysts. *Dr. Thierry Toupance* **2014**, 6–18.

(56) Minami, T.; Miyata, T.; Nishi, Y. Cu2O-Based Heterojunction Solar Cells with an Al-Doped ZnO/oxide Semiconductor/thermally Oxidized Cu2O Sheet Structure. *Sol. Energy* **2014**, *105*, 206–217.

(57) Ashok, C.; Rao, K. V.; Chakra, C. S. Facile Synthesis and Characterization of ZnO/CuO Nanocomposite for Humidity Sensor Application. *Chem. Sci. J. Adv. Chem. Sci.* **2016**, *2* (22), 223–226.

(58) Yang, C.; Cao, X.; Wang, S.; Zhang, L.; Xiao, F.; Su, X.; Wang, J. Complex-Directed Hybridization of CuO/ZnO Nanostructures and Their Gas Sensing and Photocatalytic

Properties. *Ceram. Int.* **2015**, *41* (1), 1749–1756.

(59) Sadasivam, R. K.; Mohiyuddin, S.; Packirisamy, G. Electrospun Polyacrylonitrile (PAN) Templated 2D Nanofibrous Mats: A Platform toward Practical Applications for Dye Removal and Bacterial Disinfection. *ACS Omega* **2017**, *2* (10), 6556–6569.

(60) Shavisi, Y.; Sharifnia, S.; Mohamadi, Z. Solar-Light-Harvesting Degradation of Aqueous Ammonia by CuO/ZnO Immobilized on Pottery Plate: Linear Kinetic Modeling for Adsorption and Photocatalysis Process. *J. Environ. Chem. Eng.* **2016**, *4* (3), 2736–2744.

(61) Wang, Q.; Zhang, Y.; Zheng, J.; Wang, Y.; Hu, T.; Meng, C. Metal Oxide Decorated Layered Silicate Magadiite for Enhanced Properties: Insight from ZnO and CuO Decoration. *Dalt. Trans.* **2017**, *46* (13), 4303–4316.